Global Change Biology

WILEY

Global Change Biology

RESEARCH ARTICLE

Extreme Heatwave Causes Immediate, Widespread Mortality of Forest Canopy Foliage, Highlighting Modes of Forest Sensitivity to Extreme Heat

Adam Sibley[1,2] | Christopher Still[1] | Matthew Gregory[1] | Constance Harrington[3] | David Shaw[1] | Nina Ferrari[1] | Alex Dye[1] | Mark Schulze[1] | Glenn Howe[1] | David E. Rupp[4] | Christopher Daly[5] | Daniel DePinte[6] | Cameron E. Naficy[1,7] | Chaney Hart[1] | David M. Bell[8]

[1]Department of Forest Ecosystems and Society, 321 Richardson Hall, Oregon State University, Corvallis, Oregon, USA | [2]Chloris Geospatial, Boston, Massachusetts, USA | [3]USDA Forest Service, Pacific Northwest Research Station, Olympia, WA, USA | [4]Oregon Climate Change Research Institute, College of Earth, Ocean, and Atmospheric Science, Oregon State University, Corvallis, Oregon, USA | [5]PRISM Climate Group, Northwest Alliance for Computational Science and Engineering, College of Engineering, Oregon State University, Corvallis, Oregon, USA | [6]USFS, PNW Forest Health Protection, Portland, Oregon, USA | [7]Ecology Program, Pacific Northwest Region, USDA Forest Service, Baker City, Oregon, USA | [8]USDA Forest Service, Pacific Northwest Research Station, Corvallis, Oregon, USA

Correspondence: Adam Sibley (adam@chloris.earth)

Received: 20 November 2024 | **Revised:** 11 September 2025 | **Accepted:** 29 September 2025

Funding: This research was funded by a U.S. Geological Survey Northwest Climate Adaptation Science Center (Award G17AC000218 to Adam Sibley), the H.J. Andrews Experimental Forest and Long-Term Ecological Research (LTER) program under the NSF (Grant LTER8 DEB-2025755), and USDA Forest Service Pacific Northwest Research Station.

Keywords: climate extremes | ecophysiology | foliage mortality | foliar pathogen | forest ecology | forest health | heat wave | plant thermal tolerance | remote sensing

ABSTRACT

In late June 2021, multiple days of record-breaking heat caused an unprecedented amount of foliage death in the forests of the Pacific Northwest, USA. Portions of tree canopies with healthy green foliage prior to the heat changed to red or orange shortly after the event. The change in foliage color could be readily seen in satellite imagery and was corroborated as foliar death (heat scorch) by aerial surveys and extensive observations on the ground. To better understand the patterns and processes driving foliar death, we used satellite imagery to identify 293,546 ha of forest, or ~4.7% of forest area, that were damaged in western Oregon and Washington by this extreme heat event. Analysis of underlying drivers of the observed heat damage indicated greater sensitivity was related to abiotic factors such as sun exposure, aspect, and microclimate, as well as biotic factors like tree species and stand age, budburst phenology, and foliar pathogens impacting tree health. Iconic, culturally and economically significant species like western redcedar, western hemlock, and Sitka spruce were disproportionately sensitive to heat damage, including in old-growth stands where they are canopy dominants. These findings highlight the multifaceted challenges posed to forests by extreme heat waves, and the need to better understand their impact on forest ecosystems in a rapidly warming climate.

1 | Introduction

Droughts and heatwaves exacerbated by anthropogenic climate change are anticipated to be a major driver of future forest change (Allen et al. 2015). As long-lived species that have evolved to tolerate periods of extreme weather, trees rarely die immediately in response to heat and drought; rather, forest mortality usually occurs from a combination of stressors acting over multiple years (Andrus et al. 2024; Franklin et al. 1987). While drought events impacting trees have been widely observed and

documented (e.g., Allen et al. 2010; Anderegg et al. 2013; Andrus et al. 2024; Bose et al. 2024; Hammond et al. 2022), studies examining the long-term impacts of short duration, extreme heat have been largely restricted to seedlings and laboratory studies (Fauset et al. 2019; Marias et al. 2016; Slot and Winter 2017). The effects of short, extreme heatwaves are poorly captured in most ecosystem models, and in some cases are not represented at all (Jiang et al. 2019; Kala et al. 2016). This is partly because there are multiple proposed mechanisms underlying heat stress and damage to leaves (Berry and Bjorkman 1980; Teskey et al. 2015).

Plant responses to heat stress affect many physiological processes and biological structures simultaneously. Rising temperatures initially increase photosynthesis rates until an optimum is reached, beyond which photosynthesis declines with increasing mitochondrial respiration, photorespiration, and decreasing active Rubisco and electron transport (O'Sullivan et al. 2016; Scafaro et al. 2023). Rising temperatures also limit CO_2 availability because increases in vapor pressure deficit (VPD) induce stomatal closure (Grossiord et al. 2020). Finally, direct cellular damage increases the permeability of thylakoid membranes, which disrupts photosynthetic electron transport (Sharkey 2005) and causes damage associated with oxidative bursts (Hüve et al. 2011; Zhu et al. 2024). Substantial cellular damage leads to tissue necrosis shortly after exposure to extreme heat (Colombo and Timmer 1992; Hüve et al. 2011; Javad et al. 2025; Krause et al. 2010; Marchin et al. 2022; Neuner and Buchner 2023). The connections between heat stress and tree foliar damage have been studied in controlled settings but rarely in natural environments.

Between June 25–29, 2021, an extreme heat wave occurred in the Pacific Northwest (PNW) of the United States and southwestern Canada (Loikith and Kalashnikov 2023; Mass et al. 2024; Thompson et al. 2022), which caused widespread damage to tree foliage. During this event, daily maximum air temperatures exceeded 40°C for at least three consecutive days, anomalies in maximum daily air temperature exceeded 15°C across much of the region, and all-time high temperatures were recorded in Canada (49.6°C), Washington (48.8°C), and Oregon (48.3°C) (Fleishman et al. 2025). Maximum land surface temperatures exceeded 40°C in many forested areas and exceeded 47°C in many nonforested areas (Figure 1). This heat wave was unprecedented regionally in the modern instrumentation record and had among the most extreme temperature anomalies ever recorded globally (Thompson et al. 2022). Observation and climate model-based estimates of the probability of such a heat wave occurring under the recent historical climate range widely: from 0.001% to 1.8% per year (100,000 to 56-year return interval, respectively) (Fleishman et al. 2025).

The 2021 heat wave had unprecedented effects on PNW forests. A few days after the heat wave ended, trees with dead or "scorched" foliage (Figure 2, Figures S1 and S2) appeared on the landscape as far south as Roseburg, Oregon (latitude: 43.215° N) and as far north as southern British Columbia (latitude ~49.5° N, ~700 km range). Foliage "scorch" occurs when healthy green leaves turn red, orange, or brown as living tissues die and chlorophyll is degraded due to a variety of causes. Hereafter, we use the terms foliage scorch, foliar death, leaf death, and foliar mortality interchangeably. The death of tree leaves causes an acute stress that may lead to short-term or long-term reductions in tree growth, declines in defenses, or even tree mortality, particularly if combined with stresses from other biotic and abiotic factors like co-occurring drought and pathogens.

In response to widespread reports of foliar death, the USDA Forest Service Aerial Detection Survey (ADS) conducted aerial surveys of coastal forests in northern Oregon and southern Washington. They documented ~92,000 ha of damaged forest in only a portion of the affected range (U.S. Forest Service-PNW Forest Health Protection 2023). Ground-level and aerial observations in the months after the heat wave indicated that foliar mortality was widespread but affected some forest stands more than others (Still et al. 2021). Foliar death was in some cases accompanied by mortality of branches and entire trees, with seedlings and saplings being the most sensitive (Still et al. 2021). Although it is important to understand forest sensitivity to extreme heat (Allen et al. 2015; Hammond et al. 2022; Teskey et al. 2015), to date, there has been no systematic analysis of which forests, species, or landscape positions were affected by this heatwave and why.

Initial assessments of the 2021 extreme heat wave associated forest sensitivity with biophysical factors that vary across the landscape. For example, observations suggested that temperature anomalies were important and varied geographically, that more leaf death occurred on south- and west-facing slopes, that sensitivity varied among tree species, and that vegetative phenology seemed to relate to the amount of damage (Still et al. 2023). Spatial variations in temperature anomalies during the event have been widely documented (e.g., White et al. 2023), and it is known that heat stress may be amplified or dampened by canopy position, canopy structure, aspect, and topographic position (De Frenne et al. 2021; Dobrowski 2011). The condition of the forest should also affect sensitivity to heat, especially tree water status, as well as species-specific differences in heat tolerance, tree age, and biotic stressors like foliar pathogens (Allen et al. 2015). Finally, interactions among weather, topography, and forest condition affect fine-scale variation in forest microclimate (De Frenne et al. 2019; Frey et al. 2016; Wolf et al. 2021), which could cause differentiated impacts over relatively short distances.

Our primary aim in this study was to quantify the effects of the 2021 heat event on foliar mortality in the forests of Oregon and Washington west of the Cascade mountains. First, we developed a robust, straightforward method for detecting heat-killed foliage using machine learning and satellite images acquired immediately before and after the heat wave. Next, we used geospatial datasets to determine which biophysical factors were associated with sensitivity to foliar damage across the landscape. These geospatial datasets represent factors that may mediate foliage sensitivity to extreme heat and consisted of surface and air temperatures, topographic variables, dominant tree species, canopy height, and for Douglas-fir (*Pseudotsuga menziesii*), budburst phenology and the presence of a foliar pathogen. This spatially explicit approach was used to (1) examine the associations between potential contributors to extreme heat sensitivity in these temperate, conifer-dominated forests and (2) suggest future controlled experiments or simulations to test causal relationships. Next, we identified spatial "hotspots" where mapped foliar mortality was particularly intense and evaluated the ecosystem and cultural context of two of these hotspots: old-growth forests of Olympic National Park and the plantation forests of

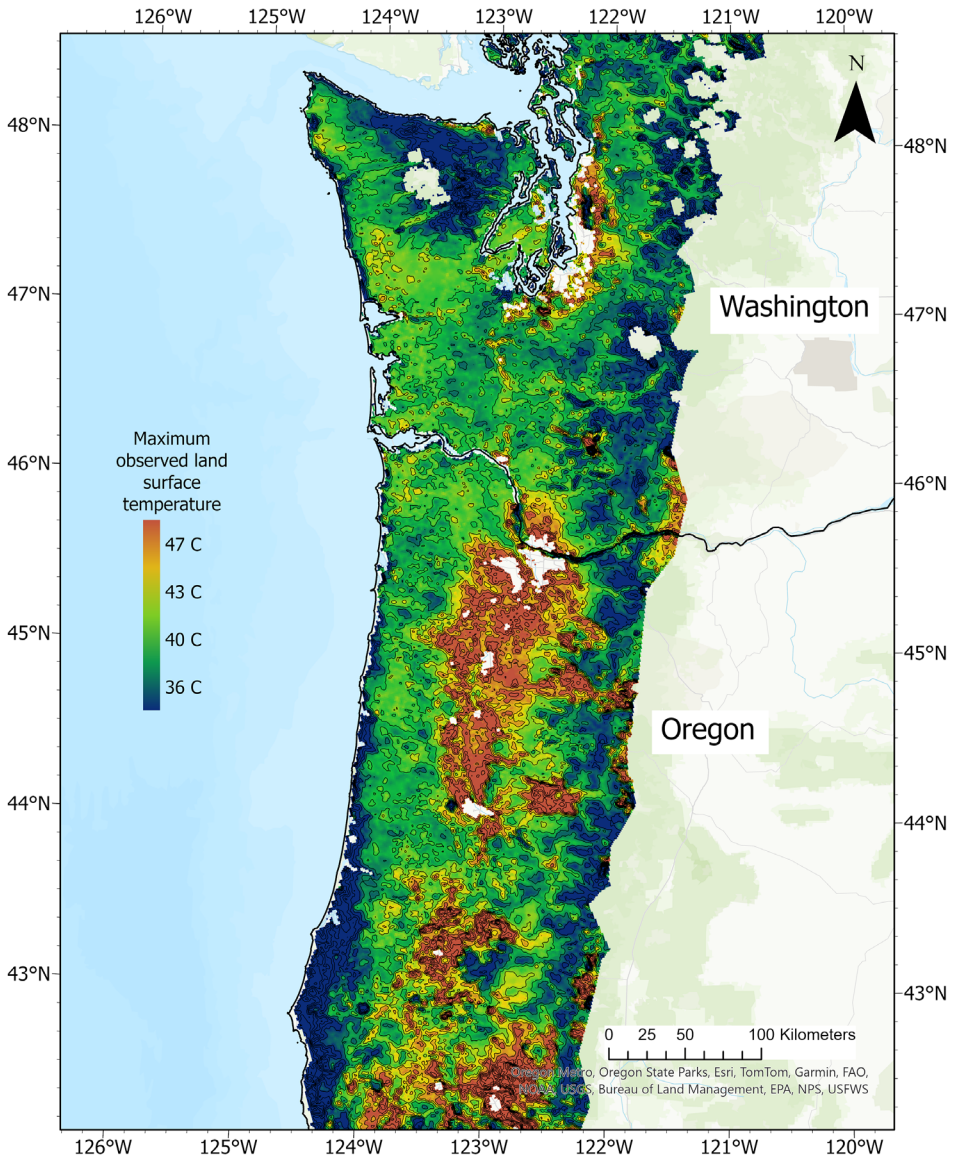

FIGURE 1 | Maximum land surface temperatures in the study area during the heatwave (June 25–29, 2021), derived from the MODIS (Moderate Resolution Imaging Spectroradiometer) daily daytime land surface temperature product (MYD11A1, Hulley and Hook 2021). Hotspots >47°C include urban areas, agricultural valleys, and burn scars from the 2020 Oregon wildfires. Isotherm line intervals are 2°C and begin at 36°C. Map lines delineate study areas and do not necessarily depict accepted national boundaries.

the Oregon Coast Range. These analyses allowed us to describe how specific heat sensitivities could lead to large future changes in forest species composition, structure, function, carbon storage, and ecosystem services if extreme heat waves become more common. Finally, we place the response of PNW forests to the 2021 heat wave in a global context and provide recommendations for further research.

2 | Materials and Methods

2.1 | Study Area

Based on communications with researchers and forestry professionals about the regional extent of canopy damage related to the 2021 heat event (Figure 2), this study focused on forested lands in the western portions of Oregon and Washington, USA (Figure 3). Forests of this area are primarily temperate coniferous forests (Franklin and Dyrness 1973). At lower elevations, dominant canopy tree species include Douglas-fir (*Pseudotsuga menziesii*), western hemlock (*Tsuga heterophylla*), and western redcedar (*Thuja plicata*). At higher elevations, dominant canopy tree species include Pacific silver fir (*Abies amabilis*) and noble fir (*Abies procera*). Deciduous tree species like Oregon white oak (*Quercus garryanna*), red alder (*Alnus rubra*), and bigleaf maple (*Acer macrophyllum*) are common in wetter valley bottoms and at the margins of non-forest ecosystems that were historically maintained by frequent fire. Other forests are locally dominated by other tree species due to particular environmental conditions, such as moisture limitation (e.g., Pacific madrone, *Arbutus menziesii*), and disturbance history, such as the presence or absence of past logging activity. By percentage of the study area where a given species has the plurality of basal area (scale: 900 m^2 grid cells, see "forest condition" section),

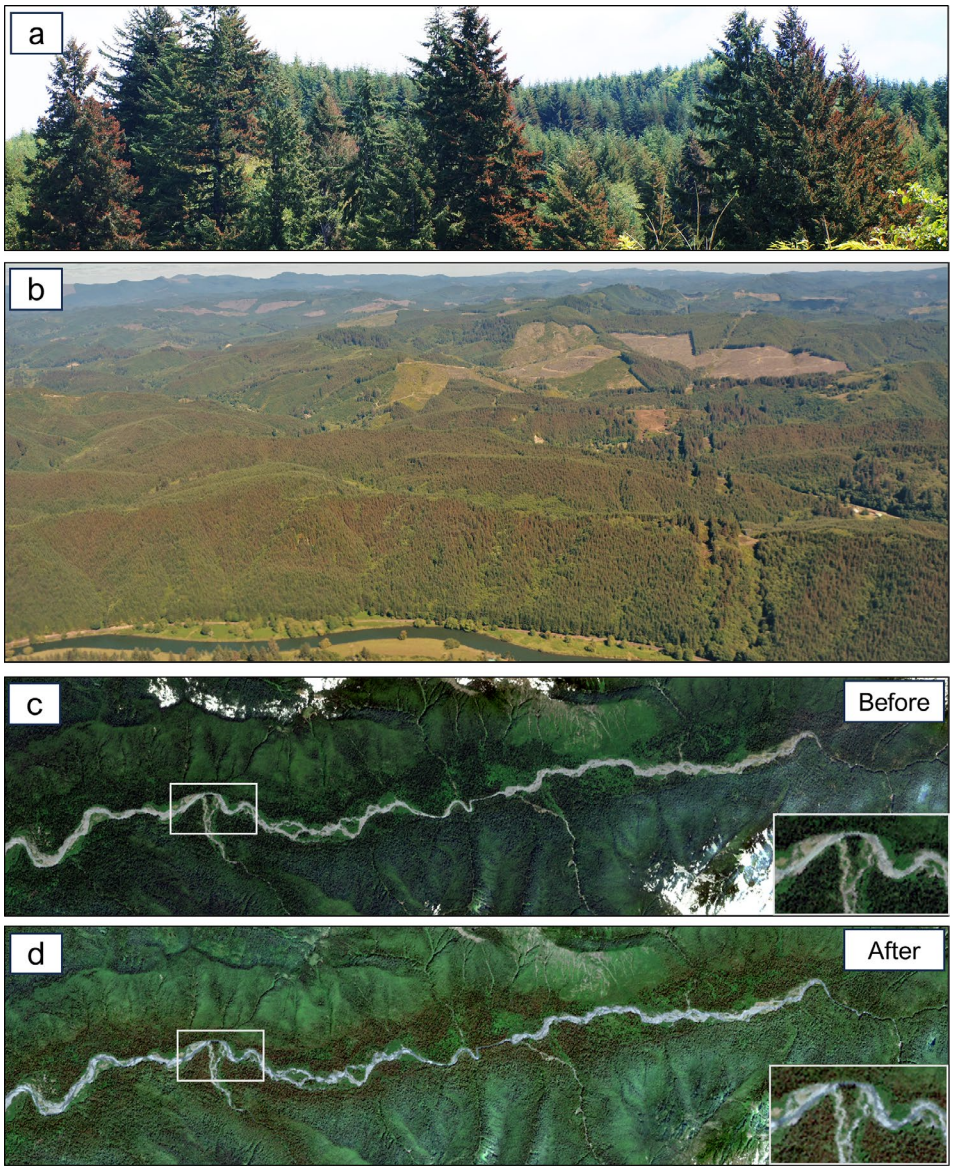

FIGURE 2 | Photographic evidence of foliar death on the landscape. (a) Douglas-fir trees near Logsden, OR (latitude: 44.74°N) with scorched foliage on west-facing branches. (b) Aerial photograph of Douglas-fir dominated hillsides near Newport, OR (credit: Daniel DePinte, latitude: 44.61°N). (c) True-color imagery composite of an upper stretch of the Hoh River on the Olympic Peninsula, WA (composite of Sentinel-2 imagery between June 1 and 24, 2021.) (d) The same stretch of the Hoh River, composite dates July 4–21, 2021. Insets in lower right show zoomed-in imagery from white boxes in the center left of the images. Notable species in this valley include Sitka spruce, bigleaf maple, western hemlock, western redcedar, red alder, and Douglas-fir.

the five most common species in the study area are Douglas-fir (*Pseudotsuga menziesii*, 65% of forest area), western hemlock (*Tsuga heterophylla* , 12.1%), red alder (*Alnus rubra* , 7.7%), western redcedar (*Thuja plicata, 3.6%*), and bigleaf maple (*Acer macrophyllum* , 3.6%) (Ohmann 2012; Bell et al. 2023). All other tree species made up the remaining 9.2% of forested area (Table 2).

2.2 | Mapping Scorch

To map forests that exhibited heat killed, or "scorched" upper-canopy foliage (that which is visible to a satellite), we gathered multispectral remote sensing data for the entire study region, collected reference data for forested pixels (scorched vs. unscorched pixels), developed a model for classifying forested pixels as scorched, and applied masking techniques to the resulting prediction maps to exclude nonforest pixels and pixels with spectral properties consistent with scorch prior to the heat event.

The imagery that we used to map scorched foliage was 10-m spatial resolution pre- and postheat wave composites of surface reflectance (SR) data from the Sentinel-2 L2A product (Copernicus Sentinel-2 (processed by ESA) 2022). We used a median composite and approximately 3 weeks of data for pre- and postheat wave intervals (June 1–24 and July 4–30, respectively), which was the minimum time range that resulted in relatively cloud-free composites and was sufficiently near in time to the event to minimize the inclusion of changes in foliage associated with other agents and/or phenological changes. Before compositing, we masked pixels that contained clouds

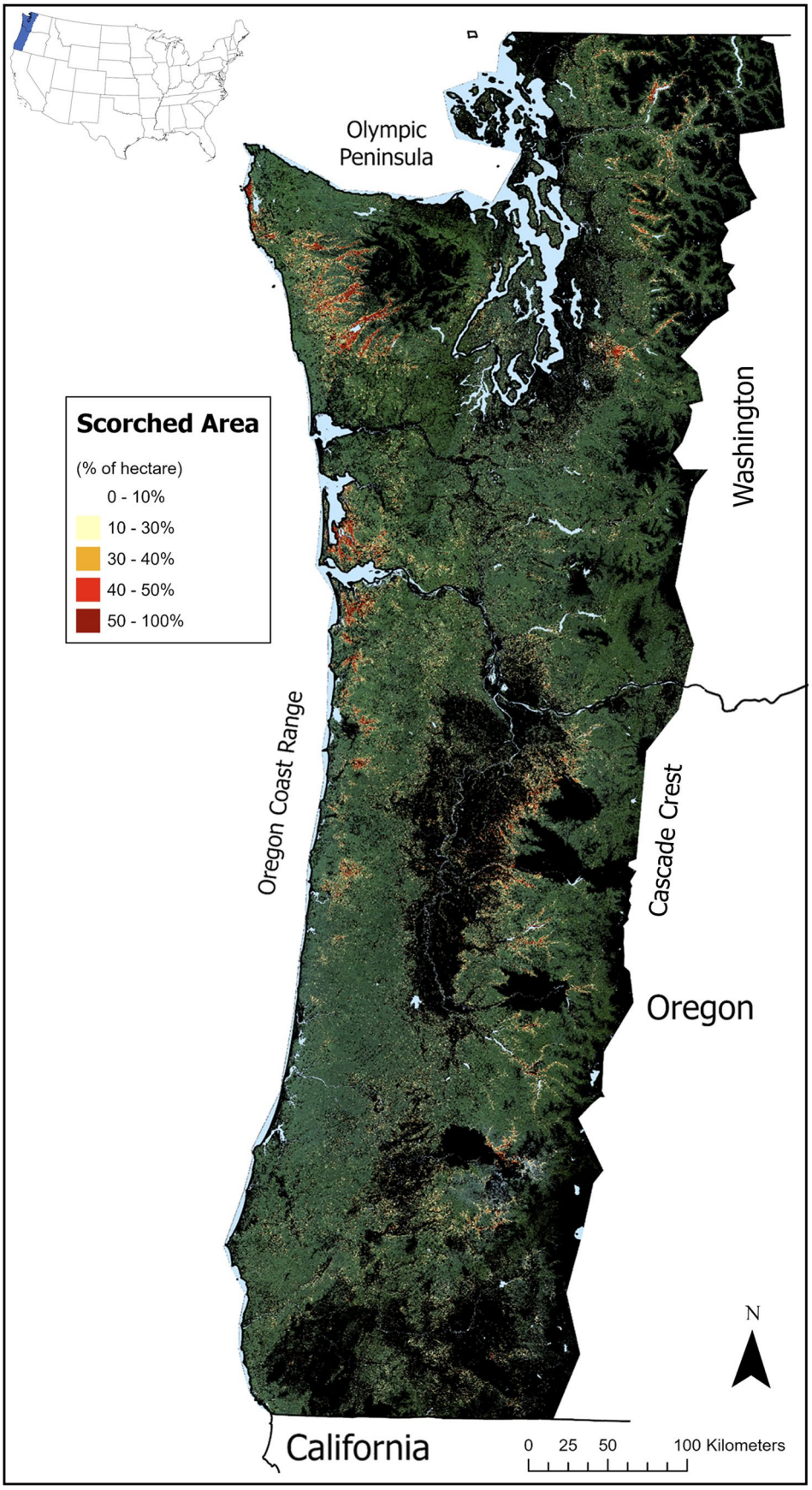

FIGURE 3 | Legend on next page.

FIGURE 3 | Map of scorched foliage, highlighting regional hotspots. Classification of scorch produced at 100 m^2 resolution was averaged over a 10,000 m^2 footprint and expressed as percent of hectare scorched. Black background represents areas that were masked out of the analysis. Green background represents areas within the study area that had < 10% canopy scorch (transparent value in legend). Inset in upper left shows study region in blue. Map lines delineate study areas and do not necessarily depict accepted national boundaries.

or cloud shadows using the "S2 Cloud Probability" layer in Google Earth Engine (GEE; Gorelick et al. 2017). Briefly, we used a cloud probability threshold of 30%, above which a pixel was excluded from consideration if its cloud displacement index was also greater than −0.5 (calculated using the GEE operator ee.Algorithms.Sentinel2.CDI) or if it had a value greater than 0.01 in Sentinel-2 band 10 (the "cirrus" band). Pixels were also masked if projected shadows intersected with low reflectance in the NIR band (band 8). We also masked pixels that had reflectance values higher than 0.035 in Sentinel-2 band 1 (the "aerosols" band) to exclude observations that were contaminated by smoke or haze, primarily from fires smoldering in southern Oregon.

To assemble a data set of training points, we used a two-stage approach. For the first stage, points of each class were chosen using Planet imagery. For areas of the Oregon Coast where substantial foliage scorch was documented in ground observations, we obtained five scene pairs of single-date (one pre-June 24, one post-July 4), high-resolution image acquisitions from Planet Scope 2 Superdove satellites (Planet Labs). These 3-m spatial resolution, true-color images from pre- and postheat wave were uploaded into GEE for training point selection. Scorch points were chosen as the centroid of a $\geq 3 \times 3$ pixel area of forest that transitioned from visibly green before the heat wave to visibly orange/red after. For a point to be labeled "unscorched," the center pixel and surrounding 3×3 area needed to be visibly green both before and after the heat wave. 971 points were selected in this way (528 scorch, 443 unscorched).

For the second stage of training data collection, an additional 354 training points were selected. Selection was done via visual inspection of true-color composites made from the pre- and postheatwave Sentinel-2 imagery described previously. We applied the same criteria of selecting the centroid of 3×3 pixel areas of either pure scorch or unscorched pixels, in this case, to avoid pixels that may be influenced by edge effects. Damaged points were selected within areas that were verified by ground observations as hotspots of canopy scorch. There were a greater number of unscorched examples selected in this round of point selection (52 scorch, 302 unscorched) as extra examples were included of locations where scorch did not occur but visible haze was present in the post-heatwave imagery near smoldering fires in southern Oregon. These points were included to improve the classification of pixels as "unscorched" when their spectral signature was influenced by haze and not tree canopy damage.

To train a random forest classifier (ee.Classifier.smileRandomForest in GEE) using these points, we extracted blue (B), green (G), red (R), and near infrared (NIR) bands from both pre- and postheat wave Sentinel image composites. For predictors, we used postheat wave composite values in the R, G, and B bands, the red to green ratio (red–green index, RGI), an index of vegetation greenness (enhanced vegetation index, EVI; Huete et al. 2002), an index of whiteness (normalized saturation-value difference index, NSVDI; Ma et al. 2008), and the difference between pre- and postheatwave composites in RGI and EVI. NSVDI was used to help counterbalance changes in band values that were caused by haze/smoke and not scorch. The classifier was configured with 50 decision trees, 3 variables per split, a minimum leaf population of 1, and a bag fraction of 0.5, which are the default settings in Google Earth Engine. Classification was done using a probability threshold of 0.5 to mimic the expectation for a binomial process.

After producing a classified map of scorch/unscorched, we applied a series of masks to ensure that further analysis only included forested areas and forest pixels which did not show signs of previous damage. To develop a mask to exclude non-forested pixels from our analysis, we used the Dynamic World near real-time land use/land cover product (Brown et al. 2022). For every pixel and every date of Sentinel-2 imagery used in our study, the Dynamic World product provided the probability that a pixel belonged to each of nine possible land cover classes. We made a preheat wave median composite of class probability values and then classified each pixel as forest or nonforest. We tested probability thresholds between 30% and 80% in increments of 10% for the "tree" class and between 5% and 30% in 5% increments for all other classes and used combinations of these thresholds to create a series of forest masks. Based on visual inspection of the study region and judging effectiveness in discriminating nonforest from forest pixels, we determined the best performing mask used criteria where pixels were considered forest if they had a median probability of belonging to the "tree" class greater than 40% as well as a lower than 15% probability of belonging to any other class. Compared to other thresholds, this combination was particularly effective at excluding forest roads and clearcut areas containing grass and shrubs. However, there remained notable cases where pixels around the perimeter of clearcuts and those making up narrow forest roads were inappropriately included in the forest class. To ensure that these areas could not be classified as scorched forest, we added a 1-pixel (10 m) square buffer to our base mask using the focal max operator in GEE, which effectively expanded the nonforest-classified areas to include these edge cases, thus eliminating them from our forest canopy scorch analyses.

In addition to the mask of nonforested areas, we developed two masks to ensure we excluded forest pixels that were orange/red before the heat wave. The first mask used the Monitoring Trends in Burn Severity (Eidenshink et al. 2007, Picotte et al. 2020, https://www.mtbs.gov/) raster product to exclude all pixels that were within the burn perimeter of a wildfire (severity class 1 or greater) that ignited in the years 2020 or 2021. This was done to exclude any trees that had been damaged in a wildfire and still retained fire-scorched dead foliage. The second mask was developed to handle all other biotic or abiotic causes of damage preheat wave. This mask was made by training a random forest

classifier on just the postheat wave composite imagery and applying it to the preheat wave composite. If a pixel was classified as "scorched" in the preheat wave imagery, it was masked from further analysis.

To validate the random forest classifier and to generate an unbiased estimate of total scorch area for our map, we used the map of scorch as a stratifier to randomly sample 349 scorch pixels and 349 unscorched pixels. The centroids of these pixels were uploaded as points to Google Earth Engine without labels. We visually interpreted change in the Sentinel-2 true-color image composites at each point location and labeled the actual scorch status for each pixel. These points were used to apply an error-adjusted area estimation approach (Olofsson et al. 2013) to generate a bias-corrected scorch area estimate with a 95% confidence interval. This approach uses an error matrix constructed for the class of interest (scorch) to quantify omission and commission rates. The total estimate of scorched area is adjusted to subtract the percentage of area represented by the commission rate and add the percentage of area represented by the omission rate. The error adjustment procedure uses a similar quantification of the omission and commission rates to quantify the standard error of the area estimate, from which the 95% confidence interval is calculated (Olofsson et al. 2013). Validation of the random forest classifier was done using the full training data set in both a hold-one-out cross-validation and a 10-fold cross-validation. Additionally, we used the training dataset together with the stratified random sample of points ($n = 1983$) to conduct a spatially blocked cross-validation using the "spatial kfold" package in Python. We used random allocation of blocks to folds, a block size of 10 km, and 15 folds to generate a mean and standard deviation of model accuracy. This method gives an accuracy estimate that is robust against spatial autocorrelation.

2.3 | Forest Scorch Related to Environmental Predictors

To quantify how the frequency of forest canopy scorch varied as a function of different potential drivers of forest sensitivity to extreme heat—specifically, geomorphology, tree species, stand height, site climatology, heat wave temperatures, and vegetative bud burst phenology—we developed a Scorch Probability Index (SPI). Within discrete intervals across the range of each data source, we calculated SPI as the proportion of mapped scorched forest area to total forest area, which demonstrates where scorch occurrence was disproportionately high relative to the existing areal coverage under a given set of conditions (e.g., for southwest-facing topographic positions). To facilitate the relevant SPI comparisons, we leveraged existing geospatial data sets to quantify terrain attributes, air and land surface temperatures, tree species dominance, forest canopy height, and tree phenology (Table 1). In the figures that present the continuous variables considered (Figures 4–7 and S4), each point in the plot represents the center value of equally sized bins that were used to discretize the continuous variable. We also delineated four "hotspots" of scorch within the study region after visual inspection of the map of canopy scorch. These hotspots were chosen based on the intensity of scorch within subregions of the study area that are biogeographically distinct (Figure S3). Scorch patterns were analyzed within these hotspots when factors specific to these biogeographic regions appeared to play a role in determining scorch severity.

2.3.1 | Terrain Features

To characterize landform types and topographically driven heat loading, we used the Ecologically Relevant Geomorphology (ERGo) data set produced by the Conservation Science Partners (CSP) (Theobald et al. 2015). This data set is available at 10-m resolution and was aggregated for analysis with other predictors to a common resolution of 30-m using nearest-neighbor resampling. From this data set, we used the Continuous Heat-Insolation Load Index (CHILI), which scales between 0 and 1 and is a "surrogate for effects of insolation and topographic shading on evapotranspiration." A CHILI value of 0 represents the coolest, most shaded landscape positions, whereas 1 indicates the most sun-exposed, warmest positions. The CHILI index was computed as a function of latitude, slope, aspect (McCune and Keon 2002), and an aspect "folding parameter" of 22°, which reflects the location of "thermal south" as 22° west of due south (the aspect where cumulative thermal loading is greatest, given that direct sun in the afternoon leads to higher maximum surface temperatures than direct sun exposure in the morning). We also used a simplified version of the CSP ERGo landforms classification to assign a descriptive characterization to landscape features (Table S1). We used a 10-m map of elevation (U.S. Geological Survey, 3D Elevation Program 10-Meter Resolution Digital Elevation Model) with the ee.Terrain.aspect function in GEE to assign aspect values to each 10-m pixel, which we resampled using nearest neighbor to 30-m resolution.

2.3.2 | Air and Land Surface Temperature

We obtained daily minimum, mean, and maximum air temperatures (T_{air}) at 800 m spatial resolution for our entire study area from the PRISM Climate Group (PRISM Climate Group, accessed 2023). Daily data for November 20, 2020, through June 31, 2021, were used to calculate maximum T_{air} during the heat wave and as input to the Douglas-fir bud burst model described in the following section. We used PRISM 30-year climate normals (1991–2020) at the same spatial resolution for the dates of the heat wave (June 25–29) to quantify the number of standard deviations above mean T_{air} maximum the daily T_{air} maximum values were during the heat wave. The daily time series and climate normals are subject to uncertainties in station data availability and spatial interpolation. As such, the PRISM gridded values should be viewed as reasonable estimates, not actual observations. Data for land surface temperature ($T_{surface}$) were obtained from the MODIS daily land surface temperature and emissivity product (Hulley and Hook 2021) and were used to examine potential maximum canopy temperatures experienced by forests during the heat wave. For each day of the heat wave, temperatures were obtained for the time points closest to midday (acquisition times across days varied between 12:00 and 13:30 local time) and only values with a quality flag of 0 ("good quality") were kept. Daily $T_{surface}$ grids were reduced to a single estimate of the highest $T_{surface}$ experienced across the duration of the heat wave.

TABLE 1 | Description of environmental attributes to be related to canopy scorch.

Attribute group	Attribute name	Attribute description
Terrain	Aspect (degrees)	Slope direction in degrees
	Continuous Heat-Insolation Load Index (CHILI)	Surrogate for effects of insolation and topographic shading on evapotranspiration (McCune and Keon 2002)
	CSP ERgo Landform	Descriptive characterization to landscape features found in the map (Theobald et al. 2015)
Temperature	Air temperature (T_{air}) maximum (°C)	Maximum observed air temperature during June 25–29, 2021 (PRISM Climate Group 2023)
	Air temperature (T_{air}) maximum anomaly (unitless)	Number of standard deviations above the long-term mean maximum air temperature observed during June 25–29, 2021 (PRISM Climate Group 2023)
	Surface temperature ($T_{surface}$) maximum (°C)	Satellite remote sensing of land surface temperature (MODIS; Hulley and Hook 2021)
Forest condition	Budbreak date	The date of budburst as the first date when both chilling and forcing requirements are met (Ford et al. 2016)
	Canopy height (m)	Tree canopy height based on Landsat imagery and GEDI lidar acquisitions (Potapov et al. 2021)
	Dominant species	Tree species with the greatest proportion of the basal area, based on gradient nearest neighbor imputed forest structure and composition mapping (Bell et al. 2021, Davis et al. 2022)
	Swiss needle cast	Locality and severity of Swiss needle cast as observed in Aerial detection surveys (U.S. Forest Service-PNW Forest Health Protection 2023)

Spatially explicit estimates of air temperature, T_{air} normals, and $T_{surface}$ could not be directly compared with the terrain features (CHILI, landform type, aspect) because of the mismatch between spatial resolutions. At a scale of 800–1000 m (800 m for PRISM T_{air} and 1 km for MODIS $T_{surface}$), a variety of aspects, landform types, CHILI values, landcover types, and tree species can exist within a given pixel. Given the spatial mismatch between terrain and vegetation features (10-m and 30-m resolution) and temperature products (800-m and 1-km resolution), when temperature relationships were analyzed, we filtered our map of damage to include only the grid cells in the T_{air} and $T_{surface}$ products that contained > 75% forest cover and compared foliar scorch as a function of temperature within species (see following section) to get a relative sense of species sensitivity to high temperatures.

2.3.3 | Forest Condition

The distribution of tree species was characterized using the 2021 version of the gradient nearest neighbor (GNN; Ohmann and Gregory 2002) forest attribute maps for Oregon and Washington (Bell et al. 2021). As applied in Oregon, Washington, and California, GNN imputes measurements from USDA Forest Service Forest Inventory and Analysis—a national forest inventory of USA forests (Burrill et al. 2024)—to all forested 30-m pixels based on the similarity between plots and pixels in terms of climate, topography, and Landsat multispectral satellite imagery (Bell et al. 2021; Davis et al. 2022). For each pixel in the map (30-m resolution), tree species are assigned using the species with the greatest proportion of the basal area as measured on the plot imputed as the nearest neighbor. Though pixel-level uncertainty of relative abundance, and thus dominance, of tree species for these maps can be high, analyses at landscape to regional levels like ours are well supported (Bell et al. 2023). Still, over- or underrepresentation of some species could bias our results. Canopy height was obtained from a global forest canopy height map (Potapov et al. 2021) produced at 30-m spatial resolution, using Global Ecosystem Dynamics Investigation (GEDI) spaceborne LIDAR data and Landsat multispectral imagery.

To test the effect of the timing of Douglas-fir spring budburst (leaf phenology) on sensitivity to damage, we used a budburst prediction model (Ford et al. 2016), which predicts the date of budburst as the first date when both chilling and forcing requirements are met. Chilling and forcing were calculated as a function of hourly temperature, beginning November 1, 2020, and running through the beginning of the heat wave (June 24, 2021). Spatially explicit estimates of daily minimum and maximum T_{air} from PRISM (see previous section) were disaggregated to hourly values using the MEteoroLOgical observation DISaggregation Tool (MELODIST) (Förster et al. 2016). Within

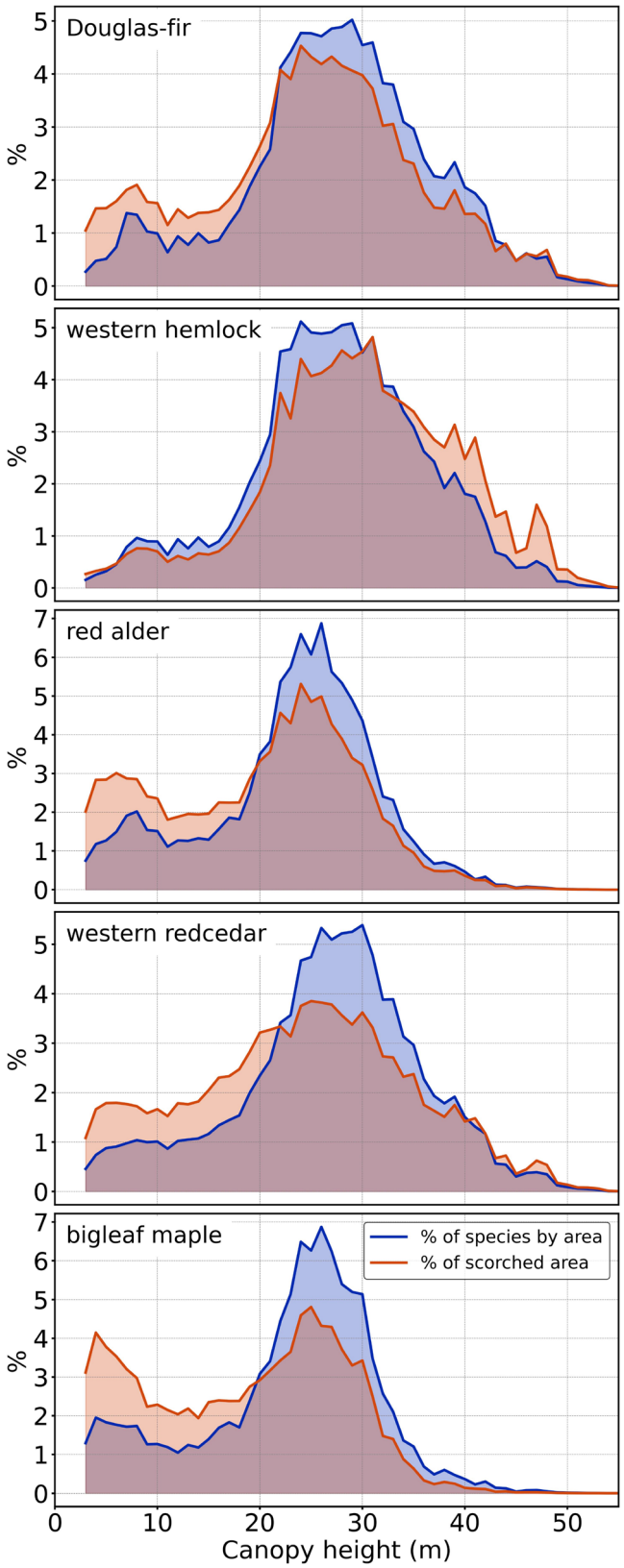

FIGURE 4 | Relationship between stand height, percent of a given species on the landscape, and percent of the scorch damaged forest within the five most common species in the study area. Canopy heights are binned at an interval of 1 m. Species labels are assigned to pixels based on the species with the greatest proportion of the basal area within the stand that the pixel represents (900 m^2 footprint).

each pixel, the first date when both chilling and forcing requirements were met was assigned to the pixel as the estimated date of budburst.

To examine the potential role of a foliar pathogen, Swiss needle cast (SNC, *Nothophaeocryptopus gaeumannii*), we incorporated into this study a map of SNC visible symptoms produced during an Aerial Detection Survey (ADS) campaign in 2018 (US Forest Service-PNW Forest Health Protection 2023). Survey flights were flown in late April to early June covering 2.7 million hectares of forest in western Oregon and Washington. Observers aboard the aircraft identified stands of Douglas-fir with yellow-brown foliage discoloration, which is a symptom of SNC infection. Polygons were drawn around affected stands and labeled as either moderately or severely infected. Both infection classes are used in this study to identify the near-coast zone of widespread SNC infection in the Coast Range (Figure 3). No explicit spatial analysis was done with these data because visible symptoms can vary from year to year within a given stand and the mapping methodology used in the survey can result in variation in mapped polygon locations between survey dates. The 2018 ADS survey was the nearest in time to the heat wave and was used in this study to identify the general zone of widespread SNC infection (Shaw et al. 2021).

2.4 | Statistical Analysis

To test the significance of relationships between scorch occurrence and potential drivers of sensitivity, we drew a spatially stratified sample of observations from the study area and used them to conduct two analyses: logistic regression and effect size quantification using Hedges' *g*. A sampling grid with ~950 m spacing was used to draw an initial sample ($n = 400{,}000$ points), within which there were 72,370 forested points. From the pool of forested pixels, we selected every dominant species type with at least 2000 points ($n = 5$) in the data set and analyzed: (1) the relationship between covariates and the probability of scorch occurrence and (2) effect sizes between the distribution of covariates for scorched and unscorched forest pixels. We did not apply denser sampling, which would have provided a sufficient sample size to examine all dominant tree species, to avoid spatial autocorrelation in the sample that could bias these statistical tests.

To quantify whether potential drivers were significantly related to increases or decreases in the probability of scorch, we fit multiple logistic regressions (using the glm function, "stats" package, R Core Team (2024)) between scorch occurrence and a single covariate for each regression: canopy height, CHILI, maximum heatwave $T_{surface}$, heatwave $T_{air\text{-}max}$, $T_{air\text{-}max}$ anomaly, and the number of standard deviations heatwave $T_{air\text{-}max}$ was above normal $T_{air\text{-}max}$. Relationships between each of these covariates and scorch within species were deemed significant if the 95% confidence interval for the estimated slope of scorch probability in logit space with respect to the covariate did not include 0.

To quantify effect sizes we calculated Hedges' g for the same covariates listed above, using the hedges_g function in the

TABLE 2 | Landscape representation and scorch damage in stands where the given species has the greatest proportion of the basal area (stand scale 900 m^2).

Species		Presence in forest		Presence in scorched forest		Scorch proportionality Index
Common name	Scientific name	Area (ha)	Percent	Area (Ha)	Percent	% of scorch: % of forest
Douglas-fir	*Pseudotsuga menziesii*	4,096,873	65.3	138,187	56.5	0.9
Western hemlock	*Tsuga heterophylla*	760,174	12.1	44,970	18.4	1.5
Red alder	*Alnus rubra*	481,115	7.7	15,719	6.4	0.8
Western redcedar	*Thuja plicata*	225,972	3.6	13,332	5.5	1.5
Bigleaf maple	*Acer macrophyllum*	225,706	3.6	9814	4.0	1.1
Pacific silver fir	*Abies amabilis*	130,631	2.1	1177	0.5	0.2
Grand fir	*Abies grandis/concolor*	52,087	0.8	1954	0.8	1.0
Sitka spruce	*Picea sitchensis*	49,261	0.8	4624	1.9	2.4
Black cottonwood	*Populus balsamifera ssp. Tric.*	32,423	0.5	1801	0.7	1.4
Oregon ash	*Fraxinus latifolia*	25,332	0.4	1882	0.8	1.9
Tanoak	*Lithocarpus densiflorus*	22,832	0.4	952	0.4	1.1
Pacific madrone	*Arbutus menziesii*	20,827	0.3	1660	0.7	2.0
Noble fir	*Abies procera/shas./magn.*	17,950	0.3	207	0.1	0.3
Umbellularia	*Umbellularia californica*	16,733	0.3	446	0.2	0.7
Lodgepole pine	*Pinus contorta*	15,807	0.3	1200	0.5	1.9
Oregon white oak	*Quercus garryana*	14,196	0.2	2501	1.0	4.5
All other species		82,034	1.3	3969	1.6	1.2
Total		6,269,953	100	244,395	100	1.0

Note: Listed species are the 16 most common species by forest area, with all remaining species grouped in "All other species". Color coding shows which species had a scorch proportionality index below 1 (blue) or above 1 (red).

"effectsize" package in R (Ben-Shachar et al. 2020). *g* values were interpreted as significant if the 95% confidence interval based on a two-tailed test did not span zero.

3 | Results

3.1 | Spatial Extent of Canopy Damage

In the 6.3 million ha of forest in our study area (western Oregon and Washington), we detected 244,395 ha of forest canopy with dead foliage (Figure 3), which is greater than 250% of the area previously reported based on spatially limited aerial surveys (U.S. Forest Service-PNW Forest Health Protection 2023). Overall accuracy of the map was 92.4% assessed using hold-one-out cross-validation, 91.2% using 10-fold cross-validation (Table S2), and 94.1% on average (standard deviation 5.5%) using spatially blocked cross-validation. Using the error-adjusted area estimation procedure given by Olofsson et al. (2013), we found that 293,546 ha were scorched (95% confidence interval = 233,674–353,418 ha), which is greater than our mapped scorch area and is consistent with omission error being greater than commission error in cross-validation results (Table S2).

3.2 | Factors Influencing Spatial Patterns of Sensitivity

The top five species by forest area—Douglas-fir (*Pseudotsuga menziesii*), western hemlock (*Tsuga heterophylla*), red alder (*Alnus rubra*), western redcedar (*Thuja plicata*), and bigleaf maple (*Acer macrophyllum)—were* also the top five species in mapped scorch area. However, the Scorch Probability Index (SPI) showed that western hemlock, western redcedar, and bigleaf maple experienced disproportionately high amounts of canopy scorch (Table 2). In contrast, Douglas-fir and red alder had an SPI below 1, indicating that the fraction of mapped scorched forest they represent is less than the fraction of total forest they represent. Notable species for their high sensitivity to heat damage were Sitka spruce (*Picea sitchensis* , SPI = 2.4), black cottonwood (*Populus trichocarpa* , SPI = 1.4), and Oregon ash (*Fraxinus latifolia* , SPI = 1.9). High-elevation species such as Pacific silver fir (*Abies amabilis* , SPI = 0.2) and noble fir (*Abies procera* , SPI = 0.3) experienced relatively little heat damage.

In addition to dominant tree species composition, forest height and phenological status also appeared to affect patterns of foliar scorch. Among four of the top five most damaged species, foliar scorch was more common in stands with shorter trees

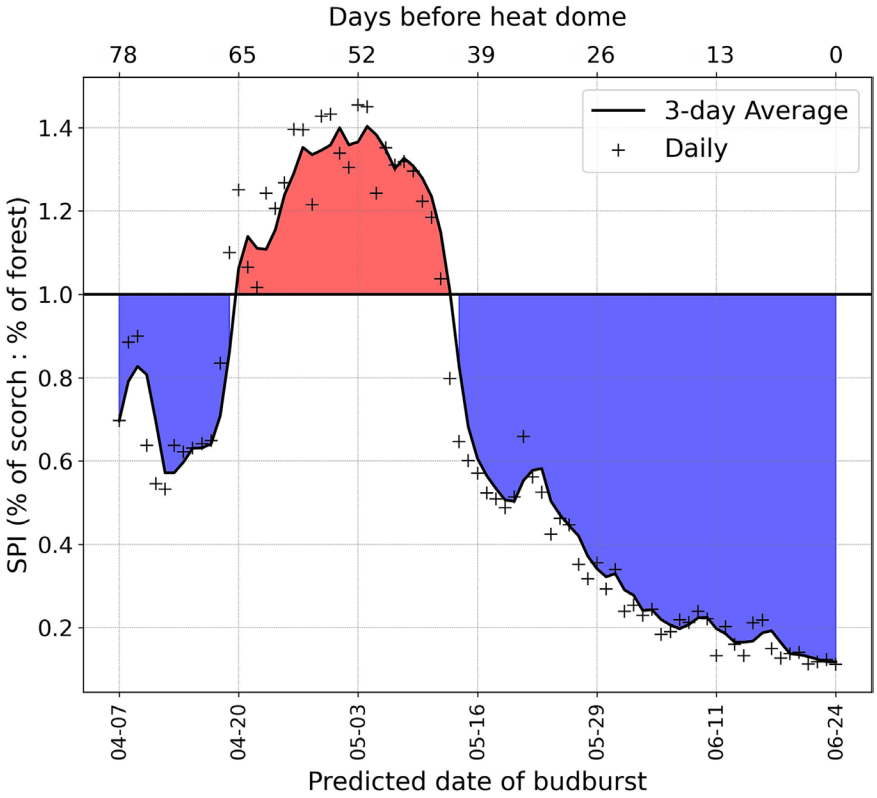

FIGURE 5 | Relationship between Scorch Proportionality Index (SPI) and predicted date of budburst in Douglas-fir.

(Figure 4). Effect sizes and logistic regression slope parameters between SPI and canopy height were negative for three of the five most common dominant tree species (Tables S3 and S4). An exception was western hemlock, which had SPI above 1 in forests with height ≥ 35 m, particularly in older forests along rivers in the western portion of the Olympic Peninsula (effect size and slope significantly positive—Tables S3 and S4). Finally, within stands dominated by Douglas-fir, trees that broke bud between April 19 and May 12 were more likely to experience damage than those that broke bud before or after those dates (Figure 5).

Across the study area, there was a tendency for higher proportions of foliar scorch (SPI > 1) on terrain positions with greater thermal loading. Specifically, mapped foliar scorch was more common when CHILI was greater than 0.63 (vertical dashed line in Figure 6a). Cooler north- and east-facing slopes largely fell under this threshold and had less scorch damage (Figure 6b,c), whereas south- and west-facing slopes were largely above this limit and made up a higher proportion of the mapped canopy scorch. CHILI values for valleys and ridge features had distinct SPI peaks at ~0.68, above the aforementioned threshold (0.63) where SPI rises above 1 (Figure 6a). Forests experiencing scorch had significantly greater CHILI values for forests dominated by three of the five most common dominant tree species (not bigleaf maple or western redcedar; Tables S3 and S4). However, valleys accounted for a larger proportion of mapped scorched forest (i.e., valleys account for 16% of the forested landscape, but 22.7% of scorched forest) than did peaks/ridges (7% of forested landscape, 6.6% of scorched forest), possibly due to the lower air temperature extremes experienced by higher elevation landscape features.

Patterns of canopy scorch within species across the range of $T_{air\text{-}max}$ and $T_{air\text{-}max}$ anomaly during the heat wave (Figure 7) showed that scorch prevalence increased above a maximum T_{air} of approximately 38°C. SPI values exceeded 1 at different thresholds for different species, with western redcedar being the most vulnerable (40°C) and bigleaf maple being the most tolerant (42.5°C). The general pattern of rising mapped scorch prevalence to SPI values greater than 1 beyond 40°C can be seen in observations of maximum $T_{surface}$ as well (Figure S4). Forests experiencing scorch had significantly greater maximum T_{air} and $T_{surface}$ for forests dominated by four of the five most common dominant tree species (no red alder; Tables S3 and S4). $T_{surface}$ values more closely correspond to sunlit leaf temperatures (T_{leaf}), which typically exceed air temperatures by 5°C–10°C (e.g., Still et al. 2023). In addition to apparent thresholds in maximum T_{leaf} and $T_{surface}$, the size of the maximum heat wave temperature anomaly was also relevant to foliar sensitivity. Heat wave air temperatures were at least 2.5 standard deviations above mean $T_{air\text{-}max}$ for the vast majority of forested areas, and across species the SPI exceeded 1 at anomalies of 3.7 standard deviations or greater (Figure 6). Forests experiencing scorch had significantly greater maximum T_{air} anomalies for forests dominated by the five most common dominant tree species, but no significant effects were noted for bigleaf maple when examining temperature anomalies as standard deviations above the mean (Tables S3 and S4). Western redcedar had a high proportion of scorch at relatively low absolute temperatures but high temperature anomalies, while in comparison bigleaf maple was relatively insensitive to the magnitude of anomalies. Instead, foliage disproportionately died in this species where it occupied low-lying landscape positions, such as valley bottoms and low hillslopes, where the heat wave led to overall higher $T_{air\text{-}max}$ (Figure 7).

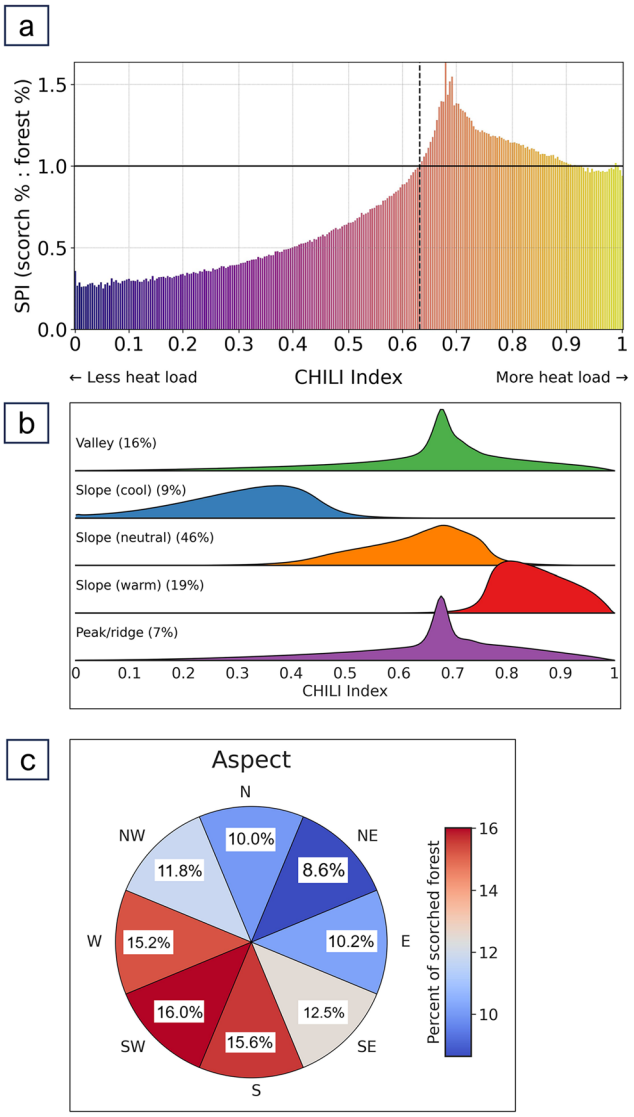

FIGURE 6 | Influence of terrain features on scorch. (a) Scorch Proportionality Index (SPI) within a given bin of the Continuous Heat-Insolation Loading Index (CHILI). Color scheme matches the scheme used in the map in Figure S6b. Distribution of CHILI values within different landform types. Percentages next to landform labels indicate the percent of the study area that falls into that landform type (see Table S1). All distributions sum to 1. (c) Percentage of scorched forest by hillslope aspect within equal area 45° slices. Nearly half of the scorched forest was within three aspects (S, SW, and W).

3.3 | Regional Variation in Canopy Scorch

Hotspots of mapped forest canopy scorch occurred in the Olympic Peninsula (49,664 ha), the Coast Range of northwest Oregon and southwest Washington (45,333 ha), and the Cascade Mountain foothills in the northern half of Oregon (35,407 ha) and in Washington (24,685 ha). Regional delineations are shown in Figure S3. On the Olympic Peninsula, damage was most extensive in Olympic National Park and Olympic National Forest, where it was conspicuously severe in the floodplain terraces and low elevation hillslopes of the river valleys west of the Olympic divide. Mapped canopy scorch was also prominent in the river valleys of the western foothills of the Cascade Mountains in both Washington and Oregon (Figure 3). In the Oregon Coast Range, which is characterized by lower elevation mountains and steeper, narrower river valleys, there was a more even balance between river valley hotspots and distributed canopy scorch on hillslopes.

4 | Discussion

The 2021 heat wave in the Pacific Northwest of North America was an uncontrolled test of the thermal tolerance of trees in their native environments. Overall, our results suggest that species distributions, species sensitivities to temperature extremes, and biotic stressors are important contributors to the unique regional hotspots of foliar mortality we observed. To our knowledge, there are no known examples of heat wave-induced foliar death at this scale in the historical record, making this event unique in the modern era. Further investigation into the specific conditions which are required to cause foliar death at this scale is merited, in anticipation of more common and more extreme future heat events.

A combination of high heat and high solar insolation can injure foliage by damaging photosystems and disrupting many aspects of photosynthesis (Teskey et al. 2015; Berry and Bjorkman 1980; Bongi and Long 1987). Foliar damage and death may also occur from membrane leakage or protein denaturation (Lancaster and Humphreys 2020; Marias et al. 2016). Because species and genotypes vary in temperature thresholds that cause foliar death (Lancaster and Humphreys 2020, Marias et al. 2016), these differences may partly explain spatial variation in foliage death. The temperature thresholds we observed (i.e., temperatures resulting in SPI > 1) were close to observed thermal limits of leaf photosystems. Irreversible damage to leaf photosystems begins at leaf temperatures above 40°C–45°C for many species (Teskey et al. 2015). Future research should aim to more precisely quantify critical thresholds (in both temperature and duration of exposure) in highly sensitive species, both in the presence and absence of high solar insolation. These studies would enhance our ability to predict the extent of foliar mortality expected under a given set of heat wave conditions and topographic variables.

Of the 10 most common tree species we studied, high scorch probability index values (SPI > 1) were observed for forests dominated by three shade-tolerant conifers (western hemlock, western redcedar, and Sitka spruce) and forests dominated by three riparian/wetland angiosperms (black cottonwood, Oregon ash, and bigleaf maple). This was surprising because these forests typically occupy geographic areas near the coast or topographic positions buffered from extremes in temperature and vapor pressure deficit (Davis et al. 2019; Dobrowski 2011) (Table 2). Thus, compared to species such as red alder and Douglas-fir, these species may not have had the same natural selection pressures for high heat tolerance. That is, they may have evolved a lower thermal threshold for damage to photosystems and other cellular structures, as well as a lower ability to resist wilting caused by uncontrolled transpiration. In contrast, upland forests dominated by Douglas-fir experienced extreme temperatures but were less sensitive to the heat wave (SPI < 1). After disturbances such as fire, this shade-intolerant, early-seral species often regenerates in high-light environments with extreme surface temperatures. Thus,

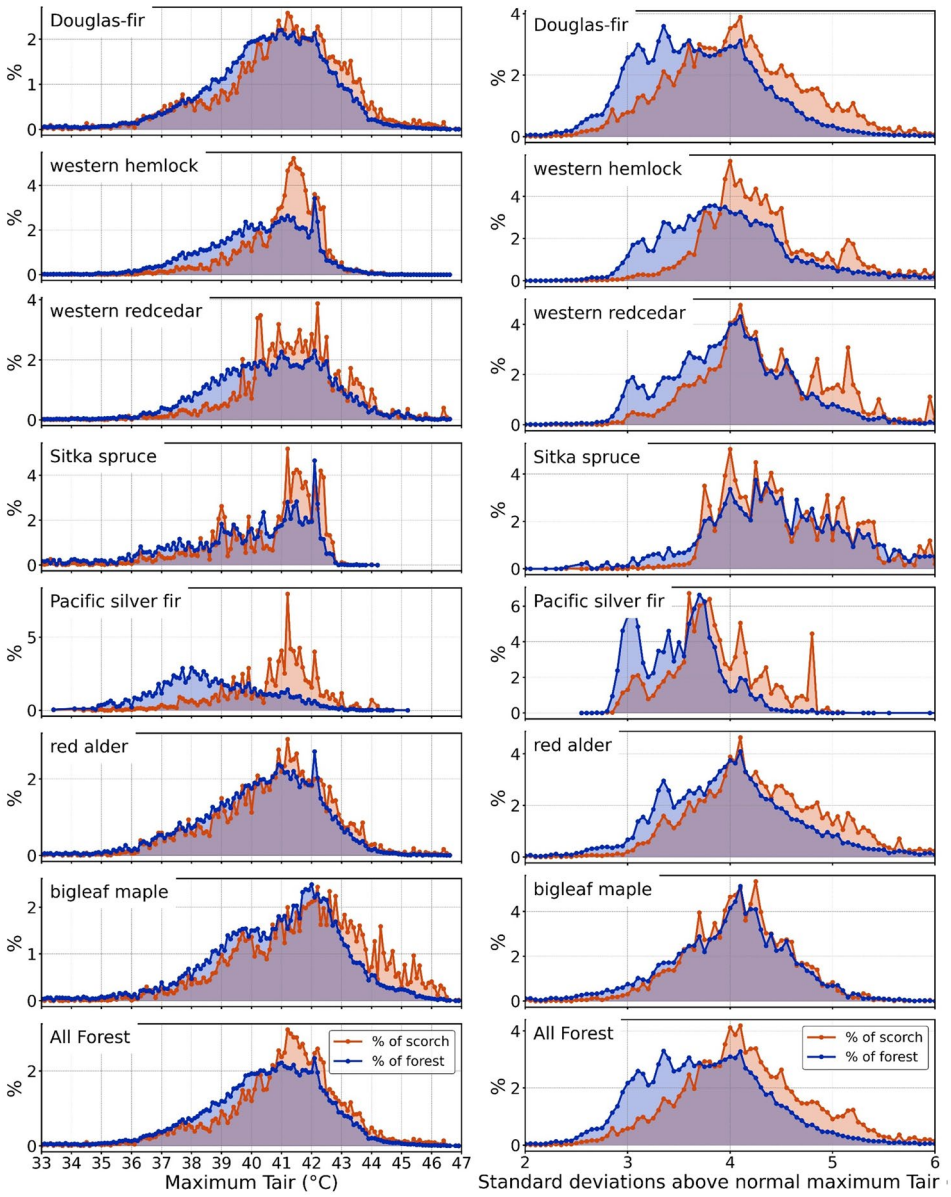

FIGURE 7 | Relationship between maximum air temperature (left column) or number of standard deviations above normal maximum T_{air} (right column) during the heat wave, the proportion of a given species on the landscape, and the proportion of the scorch damaged forest within that species. Only 800 m grid cells with > 75% forest cover were included in the analysis.

we hypothesize that low scorch resulted from natural selection for higher heat tolerance. This is also consistent with the observation that functional and morphological traits associated with leaf thermal tolerance are common in drought-tolerant tree species (Münchinger et al. 2023), since habitats that are exposed to extreme temperatures may also be drier locations. For high elevation species that also exhibited SPI < 1, canopy scorch was often observed in forests where $T_{surface\text{-}max}$ went above 40°C, but those conditions were rare for these species in our study area (see Pacific silver fir in Figure 7). Therefore, our results suggest that higher elevation species were not protected by higher thermal tolerances but rather had less exposure to high temperature extremes in the 2021 heat wave because of their topographic position (Figure 6b).

The change in canopy color due to heat-damaged foliage allowed us to explicitly map impacts across the study region. However, the heat wave may have also had negative effects on trees in areas where foliar damage was undetected (Ford et al. 2016). Heat waves that occur early in the growing season can slow growth, even when signs of stress are not apparent (Harrington et al. 2023). In Ontario, Canada, there was a spring heat wave in 2010 that coincided with leaf expansion of sugar maple trees (*Acer saccharum* Marsh.). This heat wave was associated with an earlier cessation of diameter growth, lower annual growth, and later onset of diameter growth the next year (Stangler et al. 2016). In contrast, dendrometer observations of 21 tree species across Europe showed that a late-season heat wave caused stem dehydration and temporary bole shrinkage, but no clear reduction in annual growth given that most of the seasonal growth was already completed by that time (Salomón et al. 2022). Thus, extreme heat seems to have a larger impact on tree growth when it occurs early in the growing season. In addition to reducing growth, extreme heat

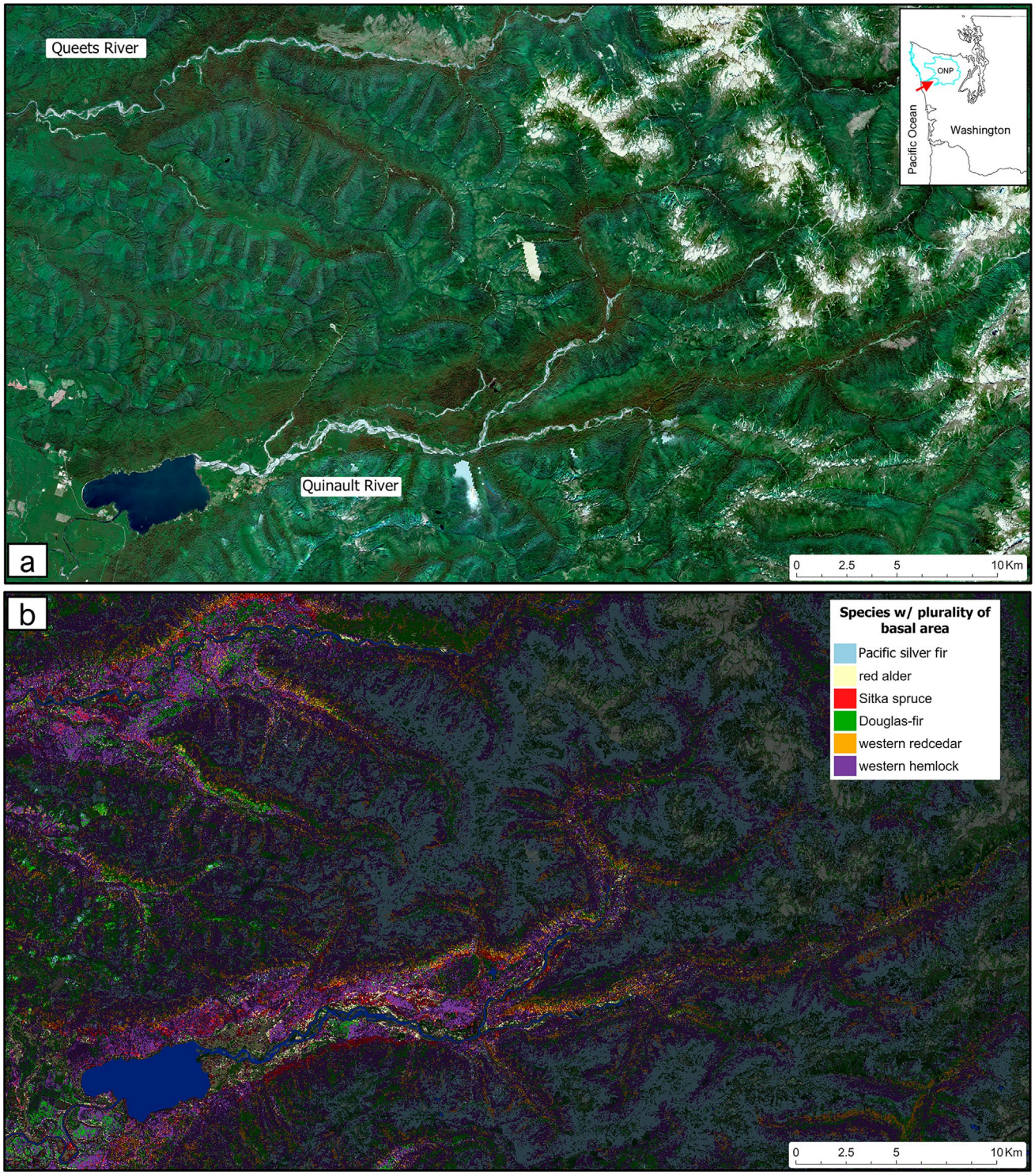

FIGURE 8 | (a) True-color median composite of the Queets and Quinault River valleys (composite period July 4–July 30), showing red/brown foliage. Inset shows Olympic National Park boundaries in blue and approximate location of image with red arrow. (b) Species map with unscorched areas partially masked with a black transparency to show contrasting species composition in scorched vs. unscorched areas.

may pre-dispose trees to damage from other biotic and abiotic stressors, ultimately leading to tree mortality after several growing seasons (Andrus et al. 2024; Franklin et al. 1987). It is still unclear whether tree mortality will increase as a result of the 2021 heat wave, or how tree growth has been impacted across the region. Future research which focuses on quantifying lasting physiological impairment or enhanced mortality rates among scorched populations of trees would lend important insight into the long-term consequences of this event.

At the local scale, species interact with unique combinations of biotic and abiotic factors that are not fully captured in regional scale analysis. In particular, tree species dominance appeared to not only play a major role in determining forest canopy scorch,

but also constrained the effects of other variables, such as canopy height (Figure 3) and temperature (Figure 6). In order to better understand more localized interactions we identified two regional scorch hotspots to describe in greater detail: Olympic National Park, where old-growth trees had extensive foliage damage, and the Oregon Coast Range, where foliage damage was mostly observed in young Douglas-fir plantations and where a foliar pathogen affecting Douglas-fir is widespread.

4.1 | Canopy Scorch in Old-Growth Forests of the Olympic National Park

We found extensive areas of foliage scorch in portions of the Olympic Peninsula, WA, including portions of the Olympic National Park (ONP), a 373,000 ha World Heritage Site and International Biosphere Reserve. The ONP contains ~150,000 ha of forest, 69% of which has been classified as old growth (Bell et al. 2023; Davis et al. 2022). Forest dominated by western hemlock (53.3%), western redcedar (10.7%), and Sitka spruce (1%) accounted for 84% of the canopy heat damage within the park. These forests were concentrated in the Humptulips, Quinault, Queets, Hoh, and Bogachiel river valleys (Figures S6 and 8). Ninety-five percent of the damage to these three species happened at elevations between 33 and 655 m, where $T_{air\text{-}max}$ was 4–5 standard deviations above average. Absolute $T_{surface\text{-}max}$ was 40°C–42°C and CHILI values tended to be high, indicating high sun exposure (Figure S6). From June to July, there may be cloud cover for 40%–50% of daylight hours in this region (Dye et al. 2020). Cloud cover provides critical shielding from direct sun and mitigates the negative effects of heat waves in other summer-dry West Coast climates (Clemesha et al. 2018). In contrast to the cooler, wetter conditions of the Olympic Peninsula, the heat wave of 2021 was associated with clear skies, high temperatures, and adiabatic heating at low elevations—conditions to which western hemlock, western redcedar, and Sitka spruce may not have been acclimated or genetically adapted. The apparent sensitivity of some old-growth forests of the ONP is concerning because of their great ecological and societal importance. The ecological and societal values of these old forests include storage of large quantities of carbon (Gray and Whittier 2014), supporting biodiversity (Spies et al. 2018), providing cooler microclimates (Wolf et al. 2021; De Frenne et al. 2019; Frey et al. 2016; Kim et al. 2022; Schowalter 2017), and acting as refugia from some high-severity fires (Gavin et al. 2003; Huff 1995). If these ancient forests experience repeated events of widespread foliage death, or if scorch impacts are exacerbated by other stressors, we may lose many of the ecological and economic benefits these forests provide.

4.2 | Canopy Scorch in Plantation Forests of the Oregon Coast Range

The mountains of the Oregon Coast Range span from southern Oregon to southwest Washington, rising to a maximum elevation of 1250 m. These mountains, known for having some of the most productive forests in the world (Diaz et al. 2018), have a large component of fast-growing, even-aged stands of Douglas-fir and western hemlock, managed on short harvest rotations (35–55 years) (Table 3). Douglas-fir, which is among the most valuable timber species worldwide, is used for plantation forestry on every forested continent (Gilson and Maguire 2021; Lavender and Hermann 2014). After the 2021 heat wave, these Douglas-fir and hemlock forests had widespread foliage scorch with notable hot spots north of Florence, OR (latitude: 43.972° N), including near-coast stretches of the Necanicum, Nehalem, Nestucca, Siletz, and Yaquina Rivers, the watersheds of several rivers that drain into Tillamook Bay, and the headlands to the north and south of the mouth of the Columbia River (Figure 9a).

The OR Coast Range has a Mediterranean climate (~8-month wet season, ~4-month dry season) but also has a pronounced rain shadow that makes areas west of the Coast Range crest wetter, cloudier, and milder than the inland Willamette Valley. Therefore, it is plausible that the lack of acclimation to high temperatures and adiabatic heating at low elevations explain why damage hotspots occurred primarily west of the Coast Range crest (Figure 9a) and near the coast (Figure 9b). In addition, leaf death was associated with the timing of budburst. Using a model to predict the timing of vegetative budburst in Douglas-fir (Ford et al. 2016), we found that foliar death was more common on trees that burst bud ~6–9 weeks before the heat wave, compared to trees that burst bud earlier or later (Figure 5). This effect was corroborated by field observations in the northern half of the Coast Range. At low-elevation sites, Still et al. (2023) noted particularly strong patterns of dead first-year foliage and tissue necrosis in expanding shoots. In contrast, Douglas-fir in the southern part of the Coast Range experienced equally high temperatures, had an earlier date of bud burst (predicted), and

TABLE 3 | Landscape representation of the six most common species in the Coast Range region, as described for Table 2.

Species	Presence in forest		Presence in scorched forest		Scorch proportionality index
Common name	Area (Ha)	Percent	Area (Ha)	Percent	% of scorch: % of forest
Douglas-fir	422,100	61.0	25,758	57.3	0.94
Western hemlock	103,583	15.0	10,802	24.0	1.61
Red alder	116,962	16.9	4,686	10.4	0.62
Western redcedar	8,050	1.2	765	1.5	1.46
Bigleaf maple	9,166	1.3	392	0.9	0.66
Sitka spruce	28,144	4.1	2,219	4.9	1.20

Note: Color coding shows which species had a scorch proportionality index below 1 (blue) or above 1 (red).

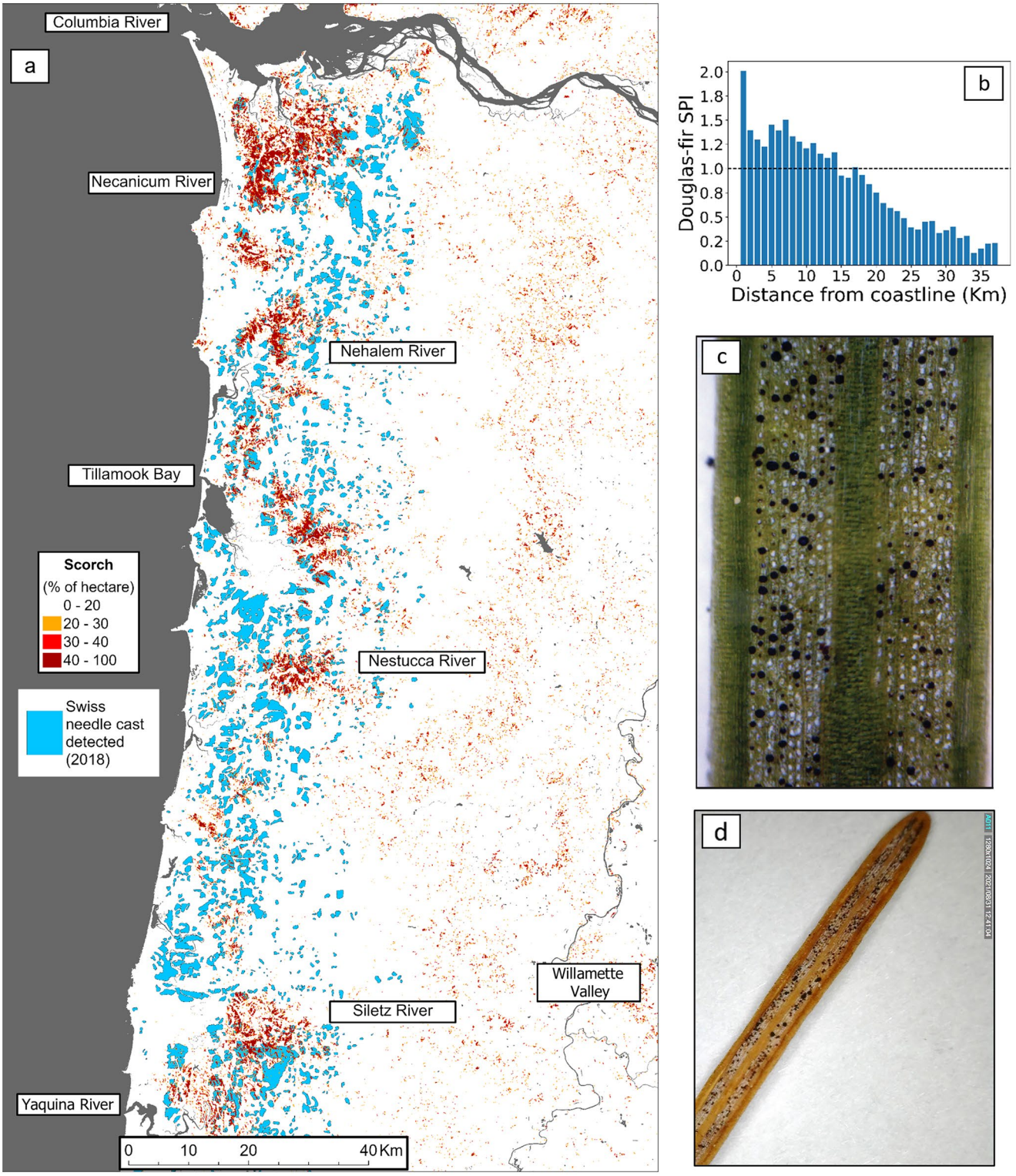

FIGURE 9 | (a) Map showing patterns of scorch in 2021 and polygons indicating where Swiss needle cast infection symptoms were observed in 2018, the time of the last Aerial Detection Survey campaign preheat wave. Visible symptoms of infection can vary in location from year to year and are displayed to illustrate the range of SNC as a function of distance from the coastline. (b) SPI of Douglas-fir as a function of distance from coastline. (c) Image of Douglas-fir needle with stoma plugged by SNC pseudothecia (photo credit: J. Schwandt). (d) Image of dead 1-year-old needle with SNC plugged stoma harvested shortly after the heat wave (credit: Gabriela Ritóková). Map lines delineate study areas and do not necessarily depict accepted national boundaries.

had less leaf damage (Figure 3). Early flushing individuals may have had an enhanced ability to resist wilting and tissue damage during the heat wave, perhaps because they were able to transport water more effectively to the new shoots, regulate leaf osmotic potential, and dissipate excess solar energy. In contrast, late budburst dates tended to occur at high elevations, where maximum heatwave T_{air} and $T_{surface}$ were lower than at low elevations, likely leading to lower SPI in these trees.

In addition to the interaction of foliar phenology and heat wave temperatures, patterns of Swiss needle cast (SNC) infection corresponded closely with scorch hotspots. SNC is a common foliage disease of Douglas-fir near the coast in Oregon and Washington (Shaw et al. 2021). The fruiting bodies of the ascomycete microfungus, *Nothophaeocryptopus gaeumannii* block needle stomata (Figure 9c), causing chronic limitation of transpiration and carbon assimilation, which leads to poor foliage retention and reduced tree growth (Manter 2002). The near-coast zone, where SNC is most prevalent (Shaw et al. 2021), had the most foliage scorch, and scorch decreased with increasing distance from the coast (Figure 9b). Trees with a history of SNC infection may have been more susceptible to foliage death in the 2021 heat wave because of generally poor health compared to more inland trees (Saffell, Meinzer, Voelker, et al. 2014; Saffell, Meinzer, Woodruff, et al. 2014). SNC may have also reduced transpirational cooling (Manter 2002), driving foliage temperatures higher than in healthy needles, increasing the probability of foliar death. This is supported by observations in the Coast Range where scorch mostly occurred on the new foliage, but in the SNC areas, scorch was also pronounced on second-year needles (fig 9d, Still et al. 2023). It remains to be seen whether the 2021 heat wave will have measurable effects on long-term productivity or mortality of Coast Range Douglas-fir.

4.3 | Extreme Heat Poses a Multifaceted Challenge to Forests

Heat and drought events have been associated with increases in tree mortality in all of Earth's major forest ecosystems (Allen et al. 2015; Hammond et al. 2022). Our work highlights the complex interactions among biotic and abiotic factors that influence forest responses to extreme heat. These interactions resulted in the complex patterns of forest canopy scorch we observed after the 2021 heat wave in the PNW. Although this heat wave was remarkably unusual, similar heat waves were responsible for record-breaking temperatures across South America in the summer of 2022 (Rivera et al. 2023). In the winter of the following year (i.e., August and September 2023), the same region experienced another heat wave. Early reporting (Kew et al. 2023) indicated that this heat wave was also characterized by record-setting, out-of-season temperatures that caused substantial damage to vegetation.

The factors that affected leaf scorch from the 2021 heat wave included maximum temperatures, temperature anomalies, degree of sun exposure, species distributions, species-specific thermal tolerances, topographic position, timing of budburst, and perhaps the presence of foliar pathogens. Our findings revealed disproportionately greater damage to some late-successional, shade-tolerant tree species, such as western hemlock and western redcedar. If heat waves increase in frequency and severity, we may see major changes in the composition of old-growth forests and reduced productivity of Coast Range plantation forests.

The effects of rare extreme events are represented poorly in the models used to project forest change, resulting in overly optimistic projections of ecosystem resistance and resilience to climate change (Allen et al. 2015; Harmon and Bell 2020). Our remote sensing approach provides a valuable starting point for quantifying the effects of heat waves and other emerging forest disturbances (Kennedy et al. 2014; McDowell et al. 2015) and could be used to understand the effects of other heat waves on forest canopies in other regions. Our results also point to new laboratory, greenhouse, and field studies that would be valuable for increasing our understanding of how extreme heat leads to ecological consequences.

Author Contributions

Adam Sibley: conceptualization, data curation, formal analysis, funding acquisition, investigation, methodology, software, supervision, validation, visualization, writing – original draft, writing – review and editing. **Christopher Still:** conceptualization, formal analysis, funding acquisition, investigation, methodology, resources, writing – original draft, writing – review and editing. **Matthew Gregory:** conceptualization, data curation, formal analysis, investigation, methodology, resources, software, validation, visualization, writing – original draft. **Constance Harrington:** conceptualization, investigation, resources, validation, writing – original draft, writing – review and editing. **David Shaw:** conceptualization, investigation, resources, writing – original draft. **Nina Ferrari:** writing – original draft. **Alex Dye:** writing – original draft. **Mark Schulze:** conceptualization, formal analysis, investigation, methodology, resources, writing – review and editing. **Glenn Howe:** funding acquisition, resources, supervision, writing – review and editing. **David E. Rupp:** data curation, investigation, investigation, resources, resources, visualization, visualization, writing – review and editing, writing – review and editing. **Christopher Daly:** conceptualization, investigation, resources. **Daniel DePinte:** data curation, investigation, resources, validation, writing – review and editing. **Cameron E. Naficy:** investigation, methodology, writing – review and editing. **Chaney Hart:** conceptualization, writing – original draft, writing – review and editing. **David M. Bell:** conceptualization, formal analysis, funding acquisition, investigation, methodology, resources, supervision, validation, visualization, writing – original draft, writing – review and editing.

Acknowledgments

We thank Dr. Kevin Ford, USDA Forest Service, for sharing R code used to predict the date of spring budburst in 2021 for Douglas-fir; Caroline Walls for her field reports of foliar heat damage on the Olympic Peninsula; and Dr. Karla M. Jarecke for her helpful editorial reviews.

Conflicts of Interest

The authors declare no conflicts of interest.

Data Availability Statement

Data produced in this study is hosted on zenodo at https://doi.org/10.5281/zenodo.17268190, along with all figures at native resolution. Code can be accessed at https://doi.org/10.5281/zenodo.17329644. The Sentinel-2 MSI L2A SR data layers used in this study can be accessed at https://doi.org/10.5270/S2_-znk9xsj. Ecologically Relevant Geomorphology (ERGo) data can be accessed at https://www.sciencebase.gov/catalog/item/561819a8e4b0cdb063e3fd96. Forest attribute maps used in this study are permanently hosted at https://lemmadownload.forestry.oregonstate.edu/ and are freely

available after filling out a data request form. PRISM climate data are available at https://doi.org/10.17616/R3S62R. MODIS Land surface temperature data can be accessed at http://doi.org/10.5067/MODIS/MOD11A1.061 and http://doi.org/10.5067/MODIS/MYD11A1.061. The 10-m resolution digital elevation model from USGS 3D elevation program can be accessed at https://doi.org/10.5069/G98K778D. Dynamic World landcover maps can be accessed at https://doi.org/10.1038/s41597-022-01307-4. Monitoring Trends in Burn Severity maps can be accessed at https://doi.org/10.5066/P9NETC0T. Swiss needle cast location data can be accessed at https://www.oregon.gov/ODF/ForestBenefits/Pages/ForestHealth.aspx.

References

Allen, C. D., D. D. Breshears, and N. G. McDowell. 2015. "On Underestimation of Global Vulnerability to Tree Mortality and Forest Die-Off From Hotter Drought in the Anthropocene." *Ecosphere* 6, no. 8: 1–55. https://doi.org/10.1890/ES15-00203.1.

Allen, C. D., A. K. Macalady, H. Chenchouni, et al. 2010. "A Global Overview of Drought and Heat-Induced Tree Mortality Reveals Emerging Climate Change Risks for Forests." *Forest Ecology and Management* 259, no. 4: 660–684. https://doi.org/10.1016/j.foreco.2009.09.001.

Anderegg, L. D. L., W. R. L. Anderegg, and J. A. Berry. 2013. "Not all Droughts Are Created Equal: Translating Meteorological Drought Into Woody Plant Mortality." *Tree Physiology* 33, no. 7: 672–683. https://doi.org/10.1093/treephys/tpt044.

Andrus, R. A., L. R. Peach, A. R. Cinquini, et al. 2024. "Canary in the Forest?—Tree Mortality and Canopy Dieback of Western Redcedar Linked to Drier and Warmer Summers." *Journal of Biogeography* 51, no. 1: 103–119. https://doi.org/10.1111/jbi.14732.

Bell, D. M., S. A. Acker, M. J. Gregory, R. J. Davis, and B. A. Garcia. 2021. "Quantifying Regional Trends in Large Live Tree and Snag Availability in Support of Forest Management." *Forest Ecology and Management* 479: 10. https://doi.org/10.1016/j.foreco.2020.118554.

Bell, D. M., M. J. Gregory, M. Palmer, and R. Davis. 2023. *Guidance for Forest Management and Landscape Ecology Applications of Recent Gradient Nearest Neighbor Imputation Maps in California, Oregon, and Washington* (No. PNW-GTR-1018; p. PNW-GTR-1018). U.S. Department of Agriculture, Forest Service, Pacific Northwest Research Station. https://doi.org/10.2737/PNW-GTR-1018.

Ben-Shachar, M., D. Lüdecke, and D. Makowski. 2020. "Effectsize: Estimation of Effect Size Indices and Standardized Parameters." *Journal of Open Source Software* 5, no. 56: 2815. https://doi.org/10.21105/joss.02815.

Berry, J., and O. Bjorkman. 1980. "Photosynthetic Response and Adaptation to Temperature in Higher Plants." *Annual Review of Plant Physiology* 31, no. 1: 491–543. https://doi.org/10.1146/annurev.pp.31.060180.002423.

Bongi, G., and S. P. Long. 1987. "Light-Dependent Damage to Photosynthesis in Olive Leaves During Chilling and High Temperature Stress." *Plant, Cell & Environment* 10, no. 3: 241–249. https://doi.org/10.1111/1365-3040.ep11602267.

Bose, A. K., J. Doležal, D. Scherrer, et al. 2024. "Revealing Legacy Effects of Extreme Droughts on Tree Growth of Oaks Across the Northern Hemisphere." *Science of the Total Environment* 926, no. 172: 49. https://doi.org/10.1016/j.scitotenv.2024.172049.

Brown, C. F., S. P. Brumby, B. Guzder-Williams, et al. 2022. "Dynamic World, Near Real-Time Global 10m Land Use Land Cover Mapping." *Scientific Data* 9, no. 1: 251. https://doi.org/10.1038/s41597-022-01307-4.

Burrill, E., A. DiTommaso, J. Turner, et al. 2024. *The Forest Inventory and Analysis Database: FIADB User Guides Volume Database Description (VERSION 9.2), Nationwide Forest Inventory (NFI)*. U.S. Department of Agriculture, Forest Service. https://www.fs.usda.gov/research/products/dataandtools/datasets/fia-datamart.

Clemesha, R. E. S., K. Guirguis, A. Gershunov, I. J. Small, and A. Tardy. 2018. "California Heat Waves: Their Spatial Evolution, Variation, and Coastal Modulation by Low Clouds." *Climate Dynamics* 50, no. 11–12: 4285–4301. https://doi.org/10.1007/s00382-017-3875-7.

Colombo, S. J., and V. R. Timmer. 1992. "Limits of Tolerance to High Temperatures Causing Direct and Indirect Damage to Black Spruce." *Tree Physiology* 11, no. 1: 95–104. https://doi.org/10.1093/treephys/11.1.95.

Copernicus Sentinel-2 (processed by ESA). 2022. *MSI Level-2A BOA Reflectance Product. Collection 1. European Space Agency*. https://doi.org/10.5270/S2_-znk9xsj.

Davis, K. T., S. Z. Dobrowski, Z. A. Holden, P. E. Higuera, and J. T. Abatzoglou. 2019. "Microclimatic Buffering in Forests of the Future: The Role of Local Water Balance." *Ecography* 42, no. 1: 1–11. https://doi.org/10.1111/ecog.03836.

Davis, R. J., D. M. Bell, M. J. Gregory, et al. 2022. *Northwest Forest Plan—The First 25 Years (1994–2018): Status and Trends of Late-Successional and Old-Growth Forests*. Pacific Northwest Research Station, USDA Forest Service, PNW-GTR-1004.

De Frenne, P., J. Lenoir, M. Luoto, et al. 2021. "Forest Microclimates and Climate Change: Importance, Drivers and Future Research Agenda." *Global Change Biology* 27, no. 11: 2279–2297. https://doi.org/10.1111/gcb.15569.

De Frenne, P., F. Zellweger, F. Rodríguez-Sánchez, et al. 2019. "Global Buffering of Temperatures Under Forest Canopies." *Nature Ecology & Evolution* 3, no. 5: 744–749. https://doi.org/10.1038/s41559-019-0842-1.

Diaz, D., S. Loreno, G. Ettl, and B. Davies. 2018. "Tradeoffs in Timber, Carbon, and Cash Flow Under Alternative Management Systems for Douglas-Fir in the Pacific Northwest." *Forests* 9, no. 8: 447. https://doi.org/10.3390/f9080447.

Dobrowski, S. Z. 2011. "A Climatic Basis for Microrefugia: The Influence of Terrain on Climate." *Global Change Biology* 17, no. 2: 1022–1035. https://doi.org/10.1111/j.1365-2486.2010.02263.x.

Dye, A. W., B. Rastogi, R. E. S. Clemesha, et al. 2020. "Spatial Patterns and Trends of Summertime Low Cloudiness for the Pacific Northwest, 1996–2017." *Geophysical Research Letters* 47, no. 16: e2020GL088121. https://doi.org/10.1029/2020GL088121.

Eidenshink, J., B. Schwind, K. Brewer, Z.-L. Zhu, B. Quayle, and S. Howard. 2007. "A Project for Monitoring Trends in Burn Severity." *Fire Ecology* 3, no. 1: 3–21. https://doi.org/10.4996/fireecology.0301003.

Fauset, S., L. Oliveira, M. S. Buckeridge, et al. 2019. "Contrasting Responses of Stomatal Conductance and Photosynthetic Capacity to Warming and Elevated CO2 in the Tropical Tree Species Alchornea Glandulosa Under Heatwave Conditions." *Environmental and Experimental Botany* 158: 28–39. https://doi.org/10.1016/j.envexpbot.2018.10.030.

Fleishman, E., D. E. Rupp, P. C. Loikith, K. A. Bumbaco, and L. W. O'Neill. 2025. "Synthesis of Publications on the Anomalous June 2021 Heat Wave in the Pacific Northwest of the United States and Canada." *Bulletin of the American Meteorological Society* 106, no. 6: E1155–E1174. https://doi.org/10.1175/BAMS-D-24-0188.1.

Ford, K. R., C. A. Harrington, S. Bansal, P. J. Gould, and J. B. St. Clair. 2016. "Will Changes in Phenology Track Climate Change? A Study of Growth Initiation Timing in Coast Douglas-Fir." *Global Change Biology* 22, no. 11: 3712–3723. https://doi.org/10.1111/gcb.13328.

Förster, K., F. Hanzer, B. Winter, T. Marke, and U. Strasser. 2016. "An Open-Source MEteoroLOgical Observation Time Series DISaggregation Tool (MELODIST v0.1.1)." *Geoscientific Model Development* 9, no. 7: 2315–2333. https://doi.org/10.5194/gmd-9-2315-2016.

Franklin, J., and C. T. Dyrness. 1973. *Natural Vegetation of Oregon and Washington*. Gen. Tech. Rep. PNW-GTR-008. Department of Agriculture, Forest Service, Pacific Northwest Research Station.

Franklin, J. F., H. H. Shugart, and M. E. Harmon. 1987. "Tree Death as an Ecological Process." *Bioscience* 37, no. 8: 550–556. https://doi.org/10.2307/1310665.

Frey, S. J. K., A. S. Hadley, S. L. Johnson, M. Schulze, J. A. Jones, and M. G. Betts. 2016. "Spatial Models Reveal the Microclimatic Buffering Capacity of Old-Growth Forests." *Science Advances* 2, no. 4: e1501392. https://doi.org/10.1126/sciadv.1501392.

Gavin, D. G., L. B. Brubaker, and K. P. Lertzman. 2003. "Holocene Fire History of a Coastal Temperate Rain Forest Based on Soil Charcoal Radiocarbon Dates." *Ecology* 84, no. 1: 186–201. https://doi.org/10.1890/0012-9658(2003)084%255B0186:HFHOAC%255D2.0.CO;2.

Gilson, L. W., and D. A. Maguire. 2021. "Drivers of Productivity Differences Between Douglas-Fir Planted Within Its Native Range in Oregon and on Exotic Sites in New Zealand." *Forest Ecology and Management* 498, no. 119: 525. https://doi.org/10.1016/j.foreco.2021.119525.

Gorelick, N., M. Hancher, M. Dixon, S. Ilyushchenko, D. Thau, and R. Moore. 2017. "Google Earth Engine: Planetary-Scale Geospatial Analysis for Everyone." *Remote Sensing of Environment* 202: 18–27. https://doi.org/10.1016/j.rse.2017.06.031.

Gray, A. N., and T. R. Whittier. 2014. "Carbon Stocks and Changes on Pacific Northwest National Forests and the Role of Disturbance, Management, and Growth." *Forest Ecology and Management* 328: 167–178. https://doi.org/10.1016/j.foreco.2014.05.015.

Grossiord, C., T. N. Buckley, L. A. Cernusak, et al. 2020. "Plant responses to rising vapor pressure deficit." *New Phytologist* 226, no. 6: 1550–1566. https://doi.org/10.1111/nph.16485.

Hammond, W. M., A. P. Williams, J. T. Abatzoglou, et al. 2022. "Global Field Observations of Tree Die-Off Reveal Hotter-Drought Fingerprint for Earth's Forests." *Nature Communications* 13, no. 1: 1761. https://doi.org/10.1038/s41467-022-29289-2.

Harmon, M. E., and D. M. Bell. 2020. "Mortality in Forested Ecosystems: Suggested Conceptual Advances." *Forests* 11, no. 5: 572. https://doi.org/10.3390/f11050572.

Harrington, C. A., P. J. Gould, and R. Cronn. 2023. "Site and Provenance Interact to Influence Seasonal Diameter Growth of *Pseudotsuga menziesii*." *Frontiers in Forests and Global Change* 6, no. 1: 173707. https://doi.org/10.3389/ffgc.2023.1173707.

Huete, A., K. Didan, T. Miura, E. P. Rodriguez, X. Gao, and L. G. Ferreira. 2002. "Overview of the Radiometric and Biophysical Performance of the MODIS Vegetation Indices." *Remote Sensing of Environment* 83, no. 1–2: 195–213. https://doi.org/10.1016/S0034-4257(02)00096-2.

Huff, M. H. 1995. "Forest Age Structure and Development Following Wildfires in the Western Olympic Mountains, Washington." *Ecological Applications* 5, no. 2: 471–483. https://doi.org/10.2307/1942037.

Hulley, G., and S. Hook. 2021. *MODIS/Terra Land Surface Temperature/3-Band Emissivity Daily L3 Global 1 km SIN Grid Day V061*. NASA EOSDIS Land Processes DAAC. https://doi.org/10.5067/MODIS/MOD21A1D.061.

Hüve, K., I. Bichele, B. Rasulov, and Ü. Niinemets. 2011. "When It Is Too Hot for Photosynthesis: Heat-Induced Instability of Photosynthesis in Relation to Respiratory Burst, Cell Permeability Changes and H_2O_2 Formation." *Plant, Cell & Environment* 34, no. 1: 113–126. https://doi.org/10.1111/j.1365-3040.2010.02229.x.

Javad, A., V. Premugh, R. Tiwari, et al. 2025. "Leaf Temperatures in an Indian Tropical Forest Exceed Physiological Limits but Durations of Exposures Are Currently Not Sufficient to Cause Lasting Damage." *Global Change Biology* 31, no. 2: e70069. https://doi.org/10.1111/gcb.70069.

Jiang, Y., J. B. Kim, A. T. Trugman, Y. Kim, and C. J. Still. 2019. "Linking Tree Physiological Constraints With Predictions of Carbon and Water Fluxes at an Old-Growth Coniferous Forest." *Ecosphere* 10, no. 4: e02692. https://doi.org/10.1002/ecs2.2692.

Kala, J., M. G. De Kauwe, A. J. Pitman, et al. 2016. "Impact of the Representation of Stomatal Conductance on Model Projections of Heatwave Intensity." *Scientific Reports* 6, no. 1: 23,418. https://doi.org/10.1038/srep23418.

Kennedy, R. E., S. Andréfouët, W. B. Cohen, et al. 2014. "Bringing an Ecological View of Change to Landsat-Based Remote Sensing." *Frontiers in Ecology and the Environment* 12, no. 6: 339–346. https://doi.org/10.1890/130066.

Kew, S., I. Pinto, L. Alves, et al. 2023. *Strong Influence of Climate Change in Uncharacteristic Early Spring Heat in South America*. Grantham Research Institute, Imperial College. https://doi.org/10.25561/106753.

Kim, H., B. C. McComb, S. J. K. Frey, D. M. Bell, and M. G. Betts. 2022. "Forest Microclimate and Composition Mediate Long-Term Trends of Breeding Bird Populations." *Global Change Biology* 28, no. 21: 6180–6193. https://doi.org/10.1111/gcb.16353.

Krause, G. H., K. Winter, B. Krause, et al. 2010. "High-Temperature Tolerance of a Tropical Tree, Ficus Insipida: Methodological Reassessment and Climate Change Considerations." *Functional Plant Biology* 37, no. 9: 890. https://doi.org/10.1071/FP10034.

Lancaster, L. T., and A. M. Humphreys. 2020. "Global Variation in the Thermal Tolerances of Plants." *Proceedings of the National Academy of Sciences* 117, no. 24: 13,580–13,587. https://doi.org/10.1073/pnas.1918162117.

Lavender, D. P., and R. K. Hermann. 2014. *Douglas-fir: The genus Pseudotsuga*. Oregon Forest Research Laboratory, Oregon State University. hdl.handle.net/1957/47168.

Loikith, P. C., and D. A. Kalashnikov. 2023. "Meteorological Analysis of the Pacific Northwest June 2021 Heatwave." *Monthly Weather Review* 151, no. 5: 1303–1319. https://doi.org/10.1175/MWR-D-22-0284.1.

Ma, H., Q. Qin, and X. Shen. 2008. "Shadow Segmentation and Compensation in High Resolution Satellite Images." *IGARSS 2008–2008 IEEE International Geoscience and Remote Sensing Symposium*, II-1036-II-1039. https://doi.org/10.1109/IGARSS.2008.4779175.

Manter, D. K. 2002. "Energy Dissipation and Photoinhibition in Douglas-Fir Needles With a Fungal-Mediated Reduction in Photosynthetic Rates." *Journal of Phytopathology* 150, no. 11–12: 674–679. https://doi.org/10.1046/j.1439-0434.2002.00801.x.

Marchin, R. M., M. Esperon-Rodriguez, M. G. Tjoelker, and D. S. Ellsworth. 2022. "Crown Dieback and Mortality of Urban Trees Linked to Heatwaves During Extreme Drought." *Science of the Total Environment* 850, no. 157: 915. https://doi.org/10.1016/j.scitotenv.2022.157915.

Marias, D. E., F. C. Meinzer, D. R. Woodruff, and K. A. McCulloh. 2016. "Thermotolerance and Heat Stress Responses of Douglas-Fir and Ponderosa Pine Seedling Populations From Contrasting Climates." *Tree Physiology, Treephys* 37: tpw117v1. https://doi.org/10.1093/treephys/tpw117.

Mass, C., D. Ovens, J. Christy, and R. Conrick. 2024. "The Pacific Northwest Heat Wave of 25–30 June 2021: Synoptic/Mesoscale Conditions and Climate Perspective." *Weather and Forecasting* 39, no. 2: 275–291. https://doi.org/10.1175/WAF-D-23-0154.1.

McCune, B., and D. Keon. 2002. "Equations for Potential Annual Direct Incident Radiation and Heat Load." *Journal of Vegetation Science* 13, no. 4: 603–606. https://doi.org/10.1111/j.1654-1103.2002.tb02087.x.

McDowell, N. G., N. C. Coops, P. S. A. Beck, et al. 2015. "Global Satellite Monitoring of Climate-Induced Vegetation Disturbances." *Trends in Plant Science* 20, no. 2: 114–123. https://doi.org/10.1016/j.tplants.2014.10.008.

Münchinger, I. K., P. Hajek, B. Akdogan, A. T. Caicoya, and N. Kunert. 2023. "Leaf Thermal Tolerance and Sensitivity of Temperate Tree Species Are Correlated With Leaf Physiological and Functional Drought Resistance Traits." *Journal of Forestry Research* 34, no. 1: 63–76. https://doi.org/10.1007/s11676-022-01594-y.

Neuner, G., and O. Buchner. 2023. "The Dose Makes the Poison: The Longer the Heat Lasts, the Lower the Temperature for Functional Impairment and Damage." *Environmental and Experimental Botany* 212: 105,395. https://doi.org/10.1016/j.envexpbot.2023.105395.

Ohmann, J. L. 2012. "Mapping Change of Older Forest With Nearest-Neighbor Imputation and Landsat Time-Series." *Forest Ecology and Management* 272: 13–25.

Ohmann, J. L., and M. J. Gregory. 2002. "Predictive Mapping of Forest Composition and Structure With Direct Gradient Analysis and Nearest- Neighbor Imputation in Coastal Oregon, U.S.A." *Canadian Journal of Forest Research* 32, no. 4: 725–741. https://doi.org/10.1139/x02-011.

Olofsson, P., G. M. Foody, S. V. Stehman, and C. E. Woodcock. 2013. "Making Better Use of Accuracy Data in Land Change Studies: Estimating Accuracy and Area and Quantifying Uncertainty Using Stratified Estimation." *Remote Sensing of Environment* 129: 122–131. https://doi.org/10.1016/j.rse.2012.10.031.

O'Sullivan, O. S., M. A. Heskel, P. B. Reich, et al. 2016. "Thermal Limits of Leaf Metabolism Across Biomes." *Global Change Biology* 23, no. 1: 209–223. https://doi.org/10.1111/gcb.13477.

Picotte, J. J., K. Bhattarai, D. Howard, et al. 2020. "Changes to the Monitoring Trends in Burn Severity Program Mapping Production Procedures and Data Products." *Fire Ecology* 16, no. 1: 16. https://doi.org/10.1186/s42408-020-00076-y.

Potapov, P., X. Li, A. Hernandez-Serna, et al. 2021. "Mapping Global Forest Canopy Height Through Integration of GEDI and Landsat Data." *Remote Sensing of Environment* 253: 112,165. https://doi.org/10.1016/j.rse.2020.112165.

PRISM Climate Group. 2023. *PRISM Weather Data*. Oregon State University. https://prism.oregonstate.edu.

R Core Team. 2024. "_R: A Language and Environment for Statistical Computing_." R Foundation for Statistical Computing, Vienna, Austria. https://www.R-project.org/.

Rivera, J. A., P. A. Arias, A. A. Sörensson, et al. 2023. "2022 Early-Summer Heatwave in Southern South America: 60 Times More Likely due to Climate Change." *Climatic Change* 176, no. 8: 102. https://doi.org/10.1007/s10584-023-03576-3.

Saffell, B. J., F. C. Meinzer, S. L. Voelker, et al. 2014. "Tree-Ring Stable Isotopes Record the Impact of a Foliar Fungal Pathogen on CO_2 Assimilation and Growth in Douglas-Fir." *Plant, Cell & Environment* 37, no. 7: 1536–1547. https://doi.org/10.1111/pce.12256.

Saffell, B. J., F. C. Meinzer, D. R. Woodruff, et al. 2014. "Seasonal Carbohydrate Dynamics and Growth in Douglas-Fir Trees Experiencing Chronic, Fungal-Mediated Reduction in Functional Leaf Area." *Tree Physiology* 34, no. 3: 218–228. https://doi.org/10.1093/treephys/tpu002.

Salomón, R. L., R. L. Peters, R. Zweifel, et al. 2022. "The 2018 European Heatwave Led to Stem Dehydration but Not to Consistent Growth Reductions in Forests." *Nature Communications* 13, no. 1: 28. https://doi.org/10.1038/s41467-021-27579-9.

Scafaro, A. P., B. C. Posch, J. R. Evans, G. D. Farquhar, and O. K. Atkin. 2023. "Rubisco Deactivation and Chloroplast Electron Transport Rates Co-Limit Photosynthesis Above Optimal Leaf Temperature in Terrestrial Plants." *Nature Communications* 14, no. 1: 2820. https://doi.org/10.1038/s41467-023-38496-4.

Schowalter, T. 2017. "Arthropod Diversity and Functional Importance in Old-Growth Forests of North America." *Forests* 8, no. 4: 97. https://doi.org/10.3390/f8040097.

Sharkey, T. D. 2005. "Effects of Moderate Heat Stress on Photosynthesis: Importance of Thylakoid Reactions, Rubisco Deactivation, Reactive Oxygen Species, and Thermotolerance Provided by Isoprene." *Plant, Cell & Environment* 28, no. 3: 269–277. https://doi.org/10.1111/j.1365-3040.2005.01324.x.

Shaw, D. C., G. Ritóková, Y.-H. Lan, et al. 2021. "Persistence of the Swiss Needle Cast Outbreak in Oregon Coastal Douglas-Fir and New Insights From Research and Monitoring." *Journal of Forestry* 119, no. 4: 407–421. https://doi.org/10.1093/jofore/fvab011.

Slot, M., and K. Winter. 2017. "Photosynthetic Acclimation to Warming in Tropical Forest Tree Seedlings." *Journal of Experimental Botany* 68, no. 9: 2275–2284. https://doi.org/10.1093/jxb/erx071.

Spies, T. A., P. A. Stine, R. A. Gravenmier, J. W. Long, and M. J. Reilly. 2018. *Synthesis of Science to Inform Land Management Within the Northwest Forest Plan area* (No. PNW-GTR-966; p. PNW-GTR-966). U.S. Department of Agriculture, Forest Service, Pacific Northwest Research Station. https://doi.org/10.2737/PNW-GTR-966.

Stangler, D. F., A. Hamann, H.-P. Kahle, and H. Spiecker. 2016. "A Heat Wave During Leaf Expansion Severely Reduces Productivity and Modifies Seasonal Growth Patterns in a Northern Hardwood Forest." *Tree Physiology, Treephys* 37, no. 1: tpw094v1. https://doi.org/10.1093/treephys/tpw094.

Still, C., A. Sibley, M. Schulze, et al. 2021. *Mini-Symposium on June 2021 Heat Dome Foliage Scorch*. Oregon State University.

Still, C. J., A. Sibley, D. DePinte, et al. 2023. "Causes of Widespread Foliar Damage From the June 2021 Pacific Northwest Heat Dome: More Heat Than Drought." *Tree Physiology* 43: 203–209. https://doi.org/10.1093/treephys/tpac143.

Teskey, R., T. Wertin, I. Bauweraerts, M. Ameye, M. A. Mcguire, and K. Steppe. 2015. "Responses of Tree Species to Heat Waves and Extreme Heat Events." *Plant, Cell & Environment* 38, no. 9: 1699–1712. https://doi.org/10.1111/pce.12417.

Theobald, D. M., D. Harrison-Atlas, W. B. Monahan, and C. M. Albano. 2015. "Ecologically-Relevant Maps of Landforms and Physiographic Diversity for Climate Adaptation Planning." *PLoS One* 10, no. 12: e0143619. https://doi.org/10.1371/journal.pone.0143619.

Thompson, V., A. Kennedy-Asser, E. Vosper, et al. 2022. "The 2021 Western North America Heat Wave Among the Most Extreme Events Ever Recorded Globally." *Science Advances* 8: eabm6860. https://doi.org/10.1126/sciadv.abm6860.

U.S. Forest Service-PNW Forest Health Protection. 2023. "Aerial Detection Surveys (ADS)." https://www.fs.usda.gov/detail/r6/forest-grasslandhealth/insects-diseases/?cid=stelprdb5286951.

White, R. H., S. Anderson, J. F. Booth, et al. 2023. "The Unprecedented Pacific Northwest Heatwave of June 2021." *Nature Communications* 14, no. 1: 727. https://doi.org/10.1038/s41467-023-36289-3.

Wolf, C., D. M. Bell, H. Kim, M. P. Nelson, M. Schulze, and M. G. Betts. 2021. "Temporal Consistency of Undercanopy Thermal Refugia in Old-Growth Forest." *Agricultural and Forest Meteorology* 307: 108520. https://doi.org/10.1016/j.agrformet.2021.108520.

Zhu, L., A. P. Scafaro, E. Vierling, et al. 2024. "Heat Tolerance of a Tropical–Subtropical Rainforest Tree Species *Polyscias Elegans*: Time-Dependent Dynamic Responses of Physiological Thermostability and Biochemistry." *New Phytologist* 241, no. 2: 715–731. https://doi.org/10.1111/nph.19356.

Supporting Information

Additional supporting information can be found online in the Supporting Information section. **Data S1:** gcb70571-sup-0001-Supinfo.pdf.

VOLUME 31 | NUMBER 11

Global Change Biology

Forest sensitivity to extreme heatwaves

WILEY

Aims and scope

Global Change Biology exists to promote understanding of the interface between all aspects of current environmental change that affects a substantial part of the globe and biological systems. Studies must concern biological systems, regardless of whether they are aquatic or terrestrial, and managed or natural environments. Both biological responses and feedbacks to change are included, and may be considered at any level of organization from molecular to biome. Studies may employ theoretical, modeling, analytical, experimental, observational, and historical approaches and should be exploratory rather than confirmatory. GCB publishes primary research articles, technical advances, GCB Reviews, research reviews, research reports, opinions, perspectives, commentaries and letters.

Journal Home Page

For submission instructions, subscription and all other information visit: http://wileyonlinelibrary.com/journal/gcb.

Open Access

Global Change Biology accepts articles for Open Access publication. Please visit https://authorservices.wiley.com/author-resources/Journal-Authors/open-access/hybrid-open-access.html for further information about Open Access.

Disclaimer

The Publisher, GCB and Editors cannot be held responsible for any errors or in any consequences arising from the use of information contained in this journal. The views and opinions expressed do not necessarily reflect those of the Publisher, GCB or Editors, neither does the publication of advertisements constitute any endorsement by the Publisher, GCB, Editors, or Authors of the products advertised. Wiley Open Access articles posted to repositories or websites are without warranty from Wiley of any kind, either express or implied, including, but not limited to, warranties of merchantability, fitness for a particular purpose, or non-infringement. To the fullest extent permitted by law Wiley disclaims all liability for any loss or damage arising out of, or in connection, with the use of or inability to use the content.

Production Editor: Dinesh Mohan (gcb@wiley.com)

Cover Image: Mountains of the Oregon Coast Range near Toledo, Oregon, photographed shortly after the June 2021 heatwave in the Pacific Northwest, USA. Dead foliage (orange) can be seen in forest stands on west-facing slopes, where Douglas-fir plantations are the predominant forest type (see Sibley et al. e70571). Photo by Daniel Depinte.